
SECTION C

A NEW PARAGENESIS FOR LATE-STAGE MINERALISATION WITHIN THE BENDIGO GOLDFIELD, CENTRAL VICTORIA, AUSTRALIA: THE LATE TIMING OF GOLD

Abstract

The relative timing of gold is intimately related to the structural evolution of the Bendigo Goldfield, Victoria, Australia, which is complex and involves five stages of deformation (D₁-D₅). A detailed investigation of economic gold occurrences within the goldfield has revealed that a four-stage mineral paragenesis, which includes gold, post-dates the volumetrically significant syn-D₂ quartz veins. A relative timing for gold corresponding to mid-D₃ is proposed on the basis of structural, microstructural and paragenetic observations. Gold primarily occurs in association with reactivated D₂ quartz vein contacts, fracture networks and stylolites, which are characteristic of deformation during D₃. Paragenetically gold co-precipitated with syn-D₃ mineral assemblages, including quartz I, carbonate II, sulphides II, muscovite and carbonate III. The late-stage mineral paragenesis defines a logical and continuous sequence of events from D₂ to D₃. D₃ may represent progressive deformation and the later stages of the Benambran Orogeny (*ca* 439-435), which if true, means that the relative timing of gold is comparable with age constraints obtained through geochronology.

Key words: Bendigo Goldfield, gold, auriferous mineralisation, late stage mineralisation.

INTRODUCTION

The Bendigo Goldfield is located within the Lachlan Fold Belt of eastern Australia (Figure 1a) and is a classic example of a structurally complex, turbidite-hosted gold deposit. Globally, similar deposits occur within the Otago Schist, New Zealand (Smith *et al.* 1996), the Meguma terrane, Nova Scotia (Ryan & Smith, 1988), the Juneau terrane, Alaska (Goldfarb *et al.* 1986) and the Dolgellau gold belt, North Wales (Shepherd & Bottrell, 1993). This type of deposit is characterised by multiple phases of deformation, structural overprinting and mineral precipitation, which can be problematic for exploration and resource evaluation unless understood well.

A number of early workers suggest that the deposition of gold within the Bendigo Goldfield postdates the major quartz bodies, sulphides and other gangue minerals (e.g. Stone, 1937; Chace, 1949). Forde (1989) also proposes a late orogenic timing for gold. However, other workers, particularly more recently, (Stillwell, 1950; Jia *et al.*, 2000; Schaub and Wilson, 2002) have suggested that gold was deposited throughout much of the deformation sequence and was simultaneous with several major phases of D₂ quartz veining. Disagreement over the relative timing of gold relates partly to the structural

framework of the goldfield, which is itself a matter of contention (Forde, 1989; Schaub & Wilson, 2002; Section A). A revised five-stage deformation chronology is proposed in Sections A & B, suggesting that the structural evolution of the goldfield is more complex than previously thought.

Since 1993, Bendigo Mining Ltd. has proceeded to re-evaluate and re-develop part of the goldfield. Current development accesses eight auriferous veins to a depth of ~800 m and presents a unique opportunity to re-examine the structurally controlled auriferous veins, which typify the central Victorian goldfields (Cox *et al.*, 1991a). This study utilises the new development to investigate economic gold occurrences associated with five auriferous quartz veins. A brief review of the regional and local geology is presented, along with a review of the mineralisation and previous ideas on the relative timing of gold. The aim of this contribution is to document the mineral paragenesis and microstructural settings associated with gold, and to determine the relative timing of gold in context with the revised deformation chronology (Sections A & B).

REGIONAL GEOLOGY

The Bendigo Goldfield is located within the Bendigo Zone (BZ; Gray, 2003), one of three fault defined structural zones within the Western Sub-province (WSP; Gray *et al.*, 1997) of the Lachlan Fold Belt (LFB; Figures 1a, b; Glen, 1992; Gray & Foster, 1998, 2004; Foster & Gray, 2000; VandenBerg *et al.*, 2000; Gray *et al.*, 2002). The geology of the WSP is dominated by a monotonous succession of deformed and metamorphosed Cambro-Ordovician to Silurian turbidites (Cas & VandenBerg, 1988; Gray & Foster, 2000; VandenBerg *et al.*, 2000; Fergusson, 2003). The metasediments are typical of medium-*P/T* (Barrovian type) conditions and predominantly exhibit prehnite-pumpellyite facies metamorphism (Cox *et al.*, 1991a; Offler *et al.*, 1998). The principal style of deformation has been described as thin-skinned crustal shortening, with the formation of a predominantly east-vergent, N-S to NW-SE striking, fold and thrust belt (Gray *et al.*, 1991; Gray & Willman, 1991a, b, c; Cox *et al.*, 1991b; Foster & Gray, 2000; Gray & Foster, 2000, 2004).

Geochronological research (Foster *et al.*, 1998; Bierlein *et al.*, 2001b, c) demonstrates that the orogenic belt formed as a result of an eastward-migrating deformation front during the Late Ordovician to Middle Devonian (*ca.* 455-385 Ma). These findings, which are in general agreement with others (e.g. Collins & Vernon, 1992; Arne *et al.*,

1998; Ramsay *et al.*, 1998) rule out a synchronous, province-wide mineralising event and instead suggest that mineralisation was episodic and associated with both regional metamorphism and the later stages of deformation (Bierlein *et al.*, 2002).

THE IMAGES ON THIS PAGE HAVE BEEN REMOVED DUE TO
COPYRIGHT RESTRICTIONS

Figure 1. A. The Lachlan Fold Belt (LFB) of southeastern Australia. Subprovinces within the LFB are shown, as are the Stawell, Bendigo and Melbourne structural zones. Adapted from Gray *et al.* (1997). B. The location of the Bendigo Goldfield within the Bendigo Zone (BZ). Adapted from Gray and Willman (1991a). C. Geological map of the Bendigo region, showing biostratigraphic units, intra-zone faults and the extent of the Bendigo Goldfield. Adapted from Johansen (2001b).

Dyke swarms and felsic to intermediate intrusions with S- and I-type affinities were emplaced during two broad intervals. The first, between ~415-395 Ma (Late Silurian to Early Devonian) occurred primarily across the Stawell Zone and south-western, western

and north-central parts of the Bendigo Zone, whilst the second, between ~385-365 Ma (Middle to Late Devonian) affected the entire Melbourne Zone, most of the Bendigo Zone and the eastern part of the Stawell Zone (Richards & Singleton, 1981; Foster *et al.*, 1998; Bierlein *et al.*, 2001b, c, d). A younger period of lamprophyre dyke emplacement has been dated at 155 Ma (Jurassic) by McDougall & Wellman (1976).

BENDIGO GEOLOGY

The Bendigo Goldfield is situated within a 9 km wide NNW trending zone of deformed, Lower to Middle Ordovician turbiditic metasediments bound by the intrazone, west-dipping Whitelaw and Sebastian thrust faults to the east and west respectively (Figure 1c). The sedimentary succession at Bendigo corresponds to part of the Castlemaine Supergroup and consists of sandstones, siltstones, shales, thin polymict conglomerates and minor cone-in-cone limestones, which exhibit rapid and distinct facies changes (Cas & VandenBerg, 1988; Sharpe & MacGeehan, 1990; Willman & Wilkinson, 1992). The turbidite cycles are 10-50 m thick, upward fining and characteristic of Bouma cycles, which suggests sedimentation in a deep-sea submarine fan environment (Cas, 1983; Sharpe & MacGeehan, 1990; Turnbull & McDermott, 1998).

Structural framework

The structural evolution of the Bendigo Goldfield is complex, with a five-stage deformation chronology proposed (D₁-D₅; Sections A & B). The five stages of deformation, which are based primarily on the recognition of overprinting tectonic foliations, are summarised below.

The first phase of deformation (D₁) recognised at Bendigo corresponds to the beginning of the Benambran Orogeny (*ca.* 439-435 Ma; VandenBerg *et al.*, 2000), with the onset of ~ENE-WSW shortening and the initial development of a regionally extensive, N-S to NW-SE trending thrust belt (e.g. Gray *et al.*, 1991). Prior to the formation of mesoscopic folds, thrust faulting, layer-parallel shearing and low-grade metamorphism formed a penetrative tectonic foliation (S₁) orientated parallel to sub-parallel with bedding (Wilson & de Hedouville, 1985; Forde, 1989; Wilson *et al.*, 1992; Schaub & Wilson, 2002; Section A).

The second phase of deformation (D_2) represents progressive ~ENE-WSW shortening. D_2 is characterised by the first generation of mesoscopic folds (F_2) and associated axial planar crenulation cleavage (S_2 ; Dunn, 1896; Whitelaw, 1914; Herman, 1923; Stone, 1937; Thomas, 1939, 1953a, b; Forde, 1989, 1991; Sharpe & MacGeehan, 1990; Cox *et al.*, 1991b; Gray & Willman, 1991a, c; Willman & Wilkinson, 1992; Wilson *et al.*, 1992; VandenBerg *et al.*, 2000; Miller *et al.*, 2001; Schaubs & Wilson, 2002; Gray, 2003; Section A). In context with the models of VandenBerg *et al.* (2000) D_2 is considered to represent the peak of deformation and metamorphism during the Benambran Orogeny.

The third phase of deformation (D_3 ; Section A) represents a period of renewed ~ENE-WSW shortening and the deformation of F_2 and S_2 with the development of conjugate kink bands. The D_3 kink bands exhibit extensional geometry (*sensu* Ramsay & Huber, 1987) and vary in size from small-scale kinks on a millimetre-scale (S_3) to large-scale kinks (F_3) at a kilometric-scale. In thin section, there is a clear coeval relationship between millimetre-scale D_3 kink bands and veinlets of quartz and muscovite. In a structural context, the timing of D_3 with respect to the models of VandenBerg *et al.* (2000) is unclear and may represent either the later stages of the Benambran Orogeny or part of the younger Tabberabberan Orogeny (*ca.* 381-377 Ma; Section A; VandenBerg *et al.*, 2000).

The fourth phase of deformation (D_4) corresponds to a subsequent period of N-S to NNE-SSW directed shortening (Forde, 1989; Sections A & B), which is characterised by NE striking, sinistral contraction kink bands (*sensu* Ramsay & Huber, 1987). The D_4 contractional kink bands are not associated with any new mineral phase(s) and predominantly occur on a millimetre-scale (S_4), although D_4 kink bands at a metre-scale (F_4) are not uncommon (Section A). D_4 may correspond to the later stages of the Tabberabberan Orogeny (Gray & Willman, 1991c; Morand *et al.*, 1997; VandenBerg *et al.*, 2000; Miller & Wilson, 2004; Section B).

The fifth phase of deformation (D_5 ; Section B) represents a period of NNW-SSE shortening and the formation of a non-penetrative foliation (S_5). S_5 is characterised by W to WNW striking dextral contractional kink bands (Section B), which may be Carboniferous in age (Powell *et al.*, 1985; Stubbley, 1990; Gray & Willman, 1991c; Goscombe *et al.*, 1994). Post-dating D_5 is a period of post-Jurassic D_2 fault reactivation and deformation (Section A). However, a tectonic foliation relating to this deformation has not been observed and the extent of the deformation remains unclear.

Mineralisation

Auriferous mineralisation at Bendigo is primarily hosted within quartz veins or according to local terminology ‘quartz reefs’, with a minor amount of disseminated gold occurring within host rock proximal to some vein contacts (Wilkinson, 1988b; Sharpe & MacGeehan, 1990; Jia *et al.*, 2000; Johansen, 2001b; Johansen *et al.*, 2003). Quartz veins occur in various structural settings and can display complex cross-sectional geometries (Chace, 1949; Thomas, 1953b; Cox *et al.*, 1991a; Schaub & Wilson, 2002). The majority of the quartz veins are barren, but any may be auriferous and of economic grade at some point along their length (Sharpe & MacGeehan, 1990). The quartz veins observed at Bendigo have been classified on the basis of their morphology, structural setting and relative timing (Figures 2, 3 & Table 1; Thomas, 1953b; Wilkinson, 1988b; Sharpe & MacGeehan, 1990; Cox *et al.*, 1991a; Schaub & Wilson, 2002). The quartz vein types are not mutually exclusive, and in some cases a single quartz body may have up to three or four names applied to parts of it on the basis of differing characteristics (e.g. saddle, leg & neck reefs; Wilkinson, 1988b).

THIS IMAGE HAS BEEN REMOVED DUE TO COPYRIGHT RESTRICTIONS

Figure 2. Schematic representation of principal reef morphologies and structural settings, not to scale. Modified from Sharpe & MacGeehan (1990), Willman & Wilkinson (1992) and Johansen (2001b).

Table 1. Summary table of the principal vein and reef types observed within the Bendigo Goldfield. Basic mineralogy and texture are presented and a relative chronology based on Section A has been attempted. The reported gold content is based on non-qualitative accounts that may reflect changing economic constraints over time; see Thomas (1953b) for a qualitative grade range.

‡ Vein thickness includes the author's own observations

Vein / Reef Classification		Typical Range of Thickness (cm) ²	Primary Mineralogy and Texture	Gold Content	Relative Timing	References	
Late-Stage veining	17	Phantom veinlets	0.2 – 0.5	Pure quartz or pure calcite	Low	Late-D ₂	Dunn (1896) ^{1, 2, 8, 13}
	16	Carbonate and/or quartz veinlets	0.2 – 5	Ankerite, minor quartz	Barren or high?		Whitelaw (1914) ^{1, 2, 4, 9}
?	15	Cross course reefs	? 2000	Massive quartz	Low – moderate		Pabst (1917) ^{2, 3, 8}
D ₂ Fault Related Veins	14	Breccia veins	20 – 200	Massive quartz, vug-druse-comb quartz, carbonate & clasts of earlier vein quartz. Sulphides: asp, py; minor po	Moderate	Syn-D ₂ faulting	Bateman (1918) ²
	13	Neck reefs	30 – 500	Massive quartz. Laminated quartz associated with faulting Sulphides: asp, py; minor po	Moderate – high		Lindgren (1920) ²
	12	Massive veins	? 200	Massive quartz, some vug-druse-comb quartz	Barren – low		Stillwell (1922) ^{2, 4, 8, 9, 13}
	11	False saddle reefs	10 – 150	Massive quartz	Moderate		Stone (1937) ^{2, 8, 9, 17}
	10	En echelon veins	1 – 30	Massive quartz	Barren – low		Chace (1949) ^{1, 2, 4, 5, 8, 9, 14, 16, 17}
	9	Fault related spur veins	0.5 – 30	Massive quartz, minor vug-druse-comb quartz Sulphides: minor asp, py; rare sph, cp, gn & po	Moderate – high		McKinstry & Ohle (1949) ¹
	8	Fault parallel veins including 'backs'	30 – 200	Laminated quartz, massive quartz, minor vug-druse-comb quartz	Moderate – high		Stillwell (1950) ^{1, 2}
D ₂ Fold Related Veins	7	Cleavage (S ₂) parallel veins	5 – 50	Massive quartz Sulphides: py, po, sph & gn	Moderate	Syn- to late-D ₂ folding	Stillwell (1953) ^{2, 9, 17}
	6	East-west striking AC veins	1 – 10	Massive quartz	Low – moderate		Thomas (1953a, b) ^{2, 3, 4, 8, 9, 13, 14, 15, 17}
	5	Fold related spur veins	3 – 20	Massive quartz, minor vug-druse-comb quartz Sulphides are sparse	Low – moderate	Syn-D ₂ folding	Cox <i>et al.</i> (1986) ^{1, 2, 8, 9}
	4	Leg reefs	10 – 150	Laminated quartz, some massive quartz & vug-druse-comb quartz Sulphides: asp, py; minor sph, cp, gn, po & boul	Moderate – high		Wilkinson (1988b) ^{1, 2, 3, 4, 8, 9, 13}
	3	Trough reefs	30 – 800		Low		Forde (1989) ^{1, 2, 3, 8, 9, 14}
	2	Saddle reefs			Moderate – high		Sharpe & MacGeehan (1990) ^{2, 3, 7, 8, 9, 11, 12, 13, 15}
Early-D ₂ veins	1	Bedding parallel laminated veins	1 – 30	Non-fibrous quartz, fibrous quartz, some massive quartz & carbonate Sulphides: py, asp; minor sph & gn Several variants proposed	Moderate – high	Pre- to syn-D ₂ folding	Cox <i>et al.</i> (1991a) ^{2, 8, 9, 10, 13}
							Willman & Wilkinson (1992) ^{1, 2, 3, 4, 8, 9}
							Jessell <i>et al.</i> (1994) ¹
							Fowler (1996) ¹
							Kwak & Roberts (1996) ³
							Fowler & Winsor (1997) ¹
							Jia <i>et al.</i> (2000) ^{1, 2, 8, 9, 12, 13, 14, 16, 17}
							Johansen (2001) ^{2, 3, 4, 8, 9, 11, 13, 15}
							Schaubs & Wilson (2002) ^{1, 2, 5, 6, 7, 8, 9, 10, 11, 13, 16}

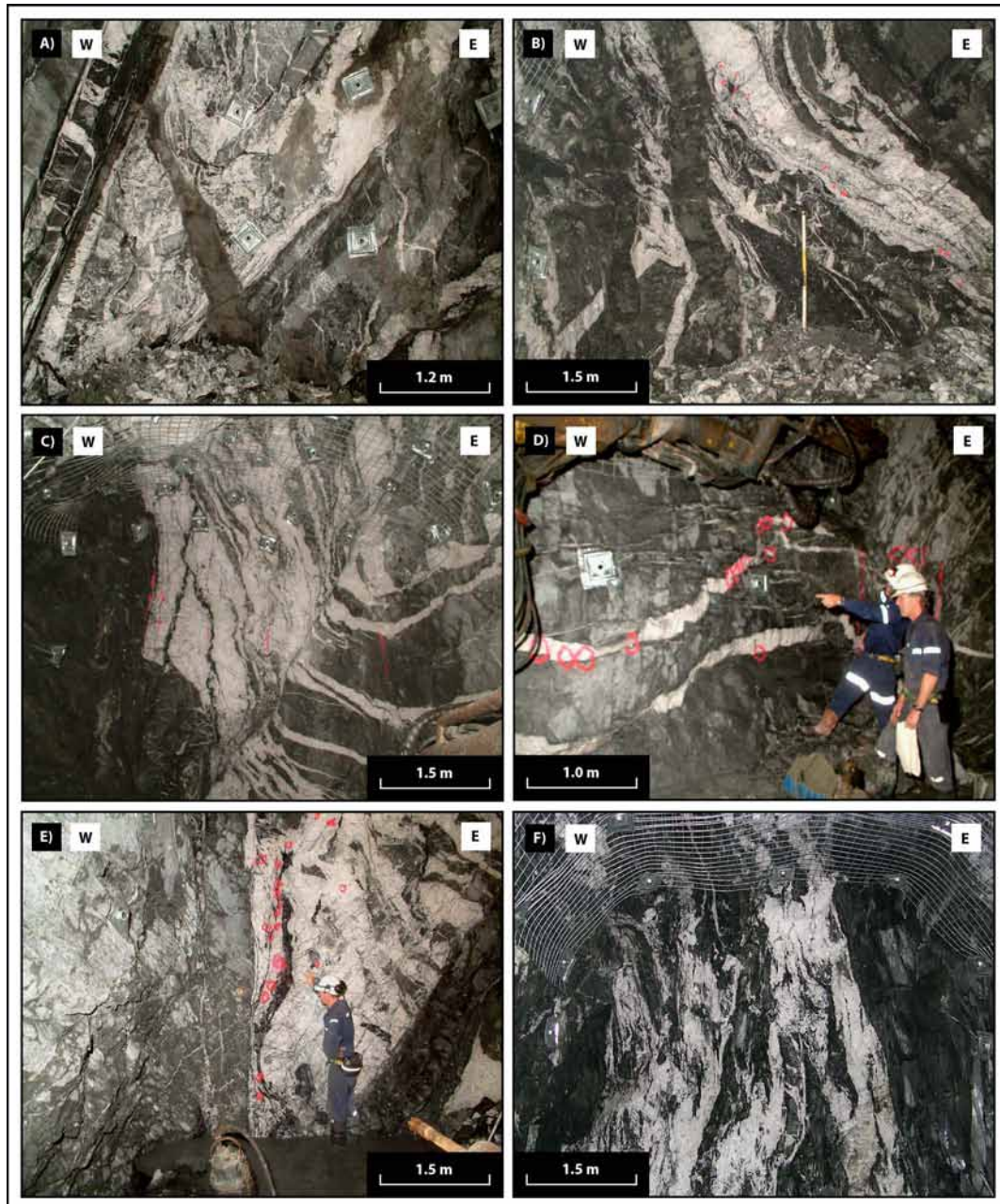


Figure 3. Auriferous quartz veins that are exposed in current underground. Pink circles and dots represent visible gold. A. Upper S3 saddle reef, west leg. Sheepshead Anticline. B. Upper S3 saddle reef, east leg. Sheepshead Anticline. C. Young's Reef, fault parallel vein. Sheepshead Anticline. D. Young's Reef, fault related spur veins. Sheepshead Anticline. E. Garrard's Reef, fault parallel vein. Sheepshead Anticline. F. D3 leg reef, east leg. Deborah Anticline. Photographs courtesy of Bendigo Mining Ltd.

Vein generations and their relative timing

Based on mineral paragenesis, metal association, vein geometry, veining events, and their crosscutting relationships Jia *et al.* (2000) recognised six main stages of veining within the Central Deborah and North Deborah deposits, which lie on the Deborah anticline (See Figures 2 & 3 in Jia *et al.*, 2000). Schaub & Wilson (2002) proposed a six stage relative chronology, which encompassed folding, faulting, vein emplacement, foliation development and the intrusion of lamprophyre dykes. This relative chronology was also based primarily on observations made in underground workings along the Deborah anticline (see Figures 3 & 5 in Schaub & Wilson, 2002).

The six stages of quartz veining proposed by Jia *et al.* (2000) and the relative chronology proposed by Schaub & Wilson (2002) are summarised in Table 2. A correlation between the work of Jia *et al.* (2000) and that of Schaub & Wilson (2002) has been attempted. The correlation relies on structural observations, vein morphology and the proposed relative timing of vein formation with respect to D₂ folding and subsequent faulting. Although the two studies focused on exposure in underground workings along the Deborah Anticline, a number of minor difficulties have been encountered. Firstly, a different number of vein types are recognised by the respective authors and secondly, the proposed timing of certain vein types relative to D₂ folding and faulting is not consistent in every case.

Vein mineralogy

Although as many as seven textural varieties of quartz have been recognised at Bendigo (Chace, 1949, p. 572-577) the veins consist predominantly of massive quartz, vug, druse and comb quartz and laminated quartz (Chace, 1949; Thomas, 1953b). Other gangue minerals include ankerite, calcite and chlorite, minor siderite, sericite and muscovite, and rare albite, apatite and sillimanite (Chace, 1949; Thomas, 1953b; Wilkinson, 1988b; Willman & Wilkinson, 1992). Ankerite is common throughout the goldfield where it occurs as ~1-12 mm thick selvages along the margins of quartz veins, and wall rock fragments and laminae contained within the quartz veins (e.g. Figures 26, 27 & 28 in Chace, 1949).

Jia <i>et al.</i> (2000)			Schaubs & Wilson (2002)			
Paragenetic Stages	Vein Types (See Table 1)	Ore Fluid Regime	Relative Chronology	Vein Types (See Table 1)	Deformation / Structure	Relative Timing
			Stage F		Intrusion of Jurassic lamprophyre dykes. Minor reactivation of faults and localised remobilisation of gold and sulphides	Post-D ₂
Stage 6	17	Late-stage hydraulic fracturing				Late-D ₂
Stage 5	16					
Stage 4	8, 13 & 14	Faulting and brittle fracturing of deposit. Fluid pressure ~165-190 MPa	Stage E		East dipping faults reactivated and west-dipping structures offset in an en echelon fashion	Syn-D ₂ faulting
Stage 3	12	Fault failure and a resulting drop in fluid pressure (~140-200 MPa)	Stage D	8 - 10, 13	Lock-up of F ₂ folds and initiation of reverse faults along pre-existing bedding-parallel veins. Spaced cleavages and crenulations develop adjacent to faults	
Stage 2	9					
			Stage C		Progressive tightening of F ₂ folds and the deformation of existing veins	Syn- to Late-D ₂ folding
Stage 1	1 - 4	Fluctuating fluid pressure (~200-300 MPa) episodically exceeds lithostatic pressure and tensile strength resulting in a crack seal process	Stage B	1 - 7	Amplification and tightening of F ₂ folds and the development of S ₂	
			Stage A	1	Initial buckling of the turbidite succession. Local small-scale thrust faulting and the possible development of an early foliation	

Table 2. Summary of the six stages of quartz veining proposed by Jia *et al.* (2000) and the six-stage relative chronology proposed by Schaubs & Wilson (2002). A correlation between the work of Jia *et al.* (2000) and that of Schaubs & Wilson (2002) is suggested in context with the deformation chronology presented in Section A.

Sulphide minerals account for ~0.5-2.5% of the ore mined at Bendigo, however, in rare instances ‘mundic lodes’ with a sulphide content of up to 30% have been encountered. The sulphide minerals include pyrite, arsenopyrite, and lesser amounts of galena, sphalerite, chalcopyrite, and pyrrhotite (Stone, 1937; Chace, 1949; Thomas, 1953b; Wilkinson, 1988b; Sharpe & MacGeehan, 1990; Willman & Wilkinson, 1992). Stibnite, pentlandite, violarite, millerite, covellite and tetrahedrite have also been reported (Chace, 1949; Thomas, 1953b; Sharpe & MacGeehan, 1990). Pyrite is typically the most abundant sulphide, though in some veins arsenopyrite may be dominant. Pyrite and arsenopyrite occur both as vein infill and wall rock alteration, whereas the other less common sulphides usually only occur as vein infill (Chace, 1949; Thomas, 1953b; Wilkinson, 1988b; c.f. Li *et al.*, 1998).

Gold occurrences

The gold at Bendigo is relatively pure with between 3 and 5% silver as the only impurity (Wilkinson, 1988b). The gold is also coarse in nature and erratically distributed within the quartz veins (Dunn, 1896; Whitelaw, 1914; Chace 1949; Thomas, 1953b; Wilkinson 1988b; Sharpe & MacGeehan, 1990; Johansen *et al.*, 2003). Gold occurs on quartz vein contacts and pressure solution features (e.g. stylolites), as free gold in massive quartz and in association with sulphides, carbonate, phantom veinlets and wall rock fragments and laminae (Chace, 1949; Thomas, 1953b; Wilkinson, 1988b; Forde, 1989; Sharpe & MacGeehan, 1990; Johansen, 2001b; Johansen *et al.*, 2003). A minor amount of gold also occurs within wall rock immediately adjacent to some auriferous quartz veins (Wilkinson, 1988b; Jia *et al.*, 2000; Johansen, 2001b).

Previous ideas on the relative timing of gold

At Bendigo, the relative timing of gold is poorly constrained, both in terms of mineral phases and the structural evolution of the goldfield. Stillwell (1922) considered “that the gold shoots are primary concentrations in the quartz reefs during the period of vein-formation”. Whereas Stone (1937, p. 890-891) reported that “veining by later quartz is characteristic of gold-bearing quartz” and that “gold and the rarer sulphides are associated with later generations of quartz”. Chace (1949, p. 592) stated that “native gold was clearly deposited later than all the gangue and sulphide minerals, with the exception of a small amount of very fine-grained late pyrite” and that “it is clearly a

very late mineral”. Chace (1949, p. 595) suggested “vein reopening and brecciation took place after the major quartz bodies had formed” and that “the effect...was to maintain permeability so that late solutions carrying some silica, sulphides and gold gained access to the otherwise solid quartz bodies”. The observations of Stone (1937) and Chace (1949) suggest that the deposition of gold occurred late in the evolution of the Bendigo system. Stillwell (1950) however, disagreed with Stone (1937) and Chace (1949), as he was unable to identify any textural differences between barren and auriferous quartz types.

Cox *et al.*, (1986) was of the opinion that “the development of auriferous quartz vein systems was broadly synchronous with regional deformation and low-grade metamorphism”. Forde (1989) who stated, “all previous models of gold-quartz vein formation have invoked only this single deformation event and have not attempted to document or differentiate between different *phases* of deformation”, proposed a three-stage deformation chronology for the Bendigo Goldfield (D₁, D₂ & D₄) and suggested that the majority of gold was hosted within breccia veins. Forde (1989, p. 8) stated “D₄ alteration both crosscuts and preferentially mineralises wall rock S₄ allowing the timing of the breccia veins, alteration and gold deposition to be defined as D₄ in age”. The D₄ structures observed at Bendigo, as reported in Sections A & B, are considered to correspond with the D₄ structures of Forde (1989). However, Sections A & B do not identify any new phases of mineral growth that can be associated with D₄ structures, which inevitably questions the D₄ timing of gold as proposed by Forde (1989).

Sharpe & MacGeehan (1990) reported that the majority of D₂ quartz veins are barren, but historically any may be auriferous and of economic grade at some point along their length. This suggests that the timing of gold post-dates the D₂ quartz veins and is associated with a later more discrete phase of mineralisation.

Cox *et al.*, (1991a) stated “vein formation and gold mineralisation locally commenced early during regional deformation” and that “gold mineralisation has clearly occurred over a protracted interval during much of the vein growth history and is not a discrete event”. Jia *et al.* (2000) recognised three stages of auriferous veining (stages 1, 2 & 4; Table 2) within the Central Deborah and North Deborah deposits. Of the three stages, stage 1 pre-dated or was syn-kinematic with D₂ folding, whereas stages 2 and 4 post-dated D₂ folding. The timing of the three stages of veining reflects their timing of

formation within the structural evolution of the goldfield (Forde, 1989; Cox *et al.*, 1991; Schaub & Wilson, 2002; Section A).

Schaub & Wilson (2002) also interpreted gold “to have precipitated throughout most of the deformation sequence” (p. 369; Table 2). Schaub & Wilson (2002, p. 369) reported that “primary gold is located in bedding-parallel veins which have not been reactivated after F_2 fold lockup, indicating that some gold was precipitated during folding” and that “the majority of the gold is contained within veins associated with D_2 faults, or in bedding-parallel veins that have been reactivated”.

This review shows that there are important disagreements about the relative timing of gold mineralisation at Bendigo. A dichotomy exists between views that significant mineralisation occurred in D_2 and later events, and views that mineralisation is only post D_2 . The distinction between D_2 and post D_2 mineralisation has fundamental significance for orogenesis, regional and near mine exploration, and resource evaluation. Part of the reason for the disagreement is that few detailed paragenetic studies (e.g. Chace, 1949) have ever been published on Bendigo; hence the rationale for this study.

SAMPLES AND THIN SECTIONS

The current underground development at Bendigo accesses eight auriferous quartz reefs on the Deborah and Sheepshead anticlines. Access was possible to five reefs, including the D3 leg reef on the Deborah Anticline and the Upper S3 saddle reef and fault related veins of Young’s reef, Christine’s reef and Garrard’s reef on the Sheepshead Anticline (Figure 3).

Approximately 50 orientated and unorientated samples were collected from the five auriferous reefs (Appendix E). In addition, a total of 4 unorientated visible-gold bearing samples were collected from Garrard’s reef and the D3 reef. A further 9 unorientated visible-gold bearing samples were collected from three successive on-lode development rounds taken from the east leg of the Upper S3 saddle reef.

Samples were cut in a plane orthogonal to structural features such as vein contacts and stylolites. The unorientated gold-bearing samples were sliced at ~10mm intervals, although a number of specific cuts were made to expose individual gold grains. In total, 52 polished thin sections and 8 standard thin sections were produced from 23 samples.

The 23 samples included samples from the five principal reef structures, as well as proximal spur veins, cleavage parallel veins and bedding parallel laminated veins.

LATE-STAGE MINERAL PARAGENESIS

A macroscopic and microscopic study of the five auriferous reefs (Figure 3) has revealed a consistent late-stage mineral paragenesis, which includes gold. The term 'late-stage' refers to episodes of mineral growth (e.g. ankerite, Chace 1949; Table 1) that post-date the D₂ quartz phases associated with D₂ folding and faulting (numbered 1-15 in Table 1). Based primarily on microscopic observations it is proposed that the late-stage mineral paragenesis consists of four stages. From oldest to youngest the stages are: (1) *sulphides I*, (2) *carbonate I*, (3) *quartz I*, *carbonate II*, *sulphides II*, *muscovite*, *gold*, and *carbonate III*, and (4) *quartz II*. Table 3 provides a summary of the late-stage paragenetic relationships.

Table 3. Summarises the significant paragenetic relationships, which are consistent within auriferous veins observed at Bendigo. A relative timing of events is presented, which is based on observations made in this section, Sections A & B. It is important to note that this study only constrains economic occurrences of gold.

Stage 1: Sulphides I

Stage 1 pyrite post-dates an earlier generation of pyrite, which pre-dates S_2 and is either a wall rock alteration or of diagenetic origin (Figure 4a; Table 3). Stage 1 sulphides consist of euhedral crystals of pyrite and arsenopyrite, both of which occur as disseminated wall rock alteration and as infill within D_2 quartz veins. Wall rock alteration arsenopyrite crystals vary greatly in size and may be up to 50 mm in diameter. Pyrite on the other hand, generally occurs as smaller crystals that are between 2 and 5 millimetres in diameter. Pyrite and arsenopyrite also occurs as discrete, fine-grained veinlets that exploit S_0 and S_2 (Figure 4b). The dominance of either pyrite or arsenopyrite appears to reflect lithology, with pyrite being more abundant within pelitic units and arsenopyrite more abundant in arenaceous units.

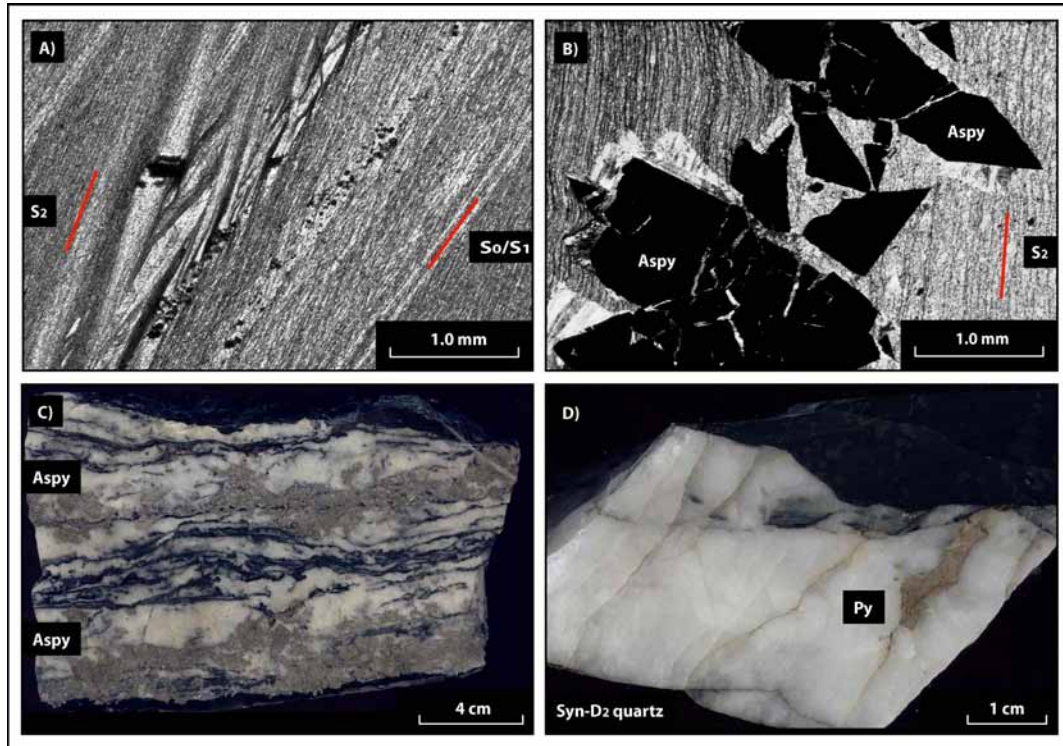


Figure 4. A. Bands of pre- S_2 pyrite crystals aligned parallel to sub-parallel with bedding (S_0). The bands of pyrite are crosscut by S_2 and strain shadows aligned parallel to S_2 are clearly evident. PPL. Thin section dips at 90° towards 345° . Sample C102. B. A band of stage I arsenopyrite (Aspy) crystals that is parallel to S_2 but which clearly post-dates S_2 . PPL. Thin section dips at 90° towards 174° . Sample G134. C. Stage I arsenopyrite (Aspy) occurring as infill within a narrow laminated D_2 quartz vein. The stage I arsenopyrite truncates the stylolitic laminations. Lower east leg, Upper S_3 saddle reef. Sample S3I. Unorientated. D. Section through a narrow bedding parallel D_2 quartz vein, which is overprinted by fractures and fracture-hosted pyrite. D3 leg reef, Deborah Anticline. Sample D3X015. Unorientated.

Within the D₂ quartz veins arsenopyrite and pyrite occur as infill and may be associated with wall rock laminae, stylolites and occasionally fractures (Figures 4c, d). Aggregates of pyrite and arsenopyrite are a common feature and commonly occur proximal to vein contacts and on well-developed stylolites. Coarse aggregates of arsenopyrite comprising crystals of up to 20 mm in diameter are common within some D₂ quartz veins.

Stage 2: Carbonate I

Carbonate I is the most abundant of the late-stage minerals and occurs predominantly as infill along reactivated D₂ quartz vein contacts, and in particular, brecciated contacts where the carbonate cements fragments of wall rock and D₂ quartz (Figure 5a). Carbonate I may also be observed within D₂ quartz veins, where it occurs in association with stylolites, fracture networks and wall rock fragments and laminae. The occurrence of carbonate I in these settings bears no relationship to the gold content of the D₂ quartz veins.

Within the host sediments carbonate I occurs as pressure fringes on stage 1 arsenopyrite and pyrite, and as 0.5-1.5mm wide veinlets that truncate S₂, but are pre-S₃ and commonly associated with the development of flanking structures (Section B; Passchier, 2001; Grasemann & Stüwe, 2001). Carbonate I also occurs as wall rock alteration in the form of second-generation carbonate spots, which encircle syn-S₂ carbonate spots that are associated with an early carbonate-bearing mineral phase (Figure 5b; Table 3; c.f. Cox *et al.*, 1991a; Kwak & Li, 1996; Li *et al.*, 1998; Bierlein *et al.*, 1998).

In hand specimen carbonate I is typically milky-white in colour, although minor gradational changes to a greyish-white are not uncommon (Figure 5a). In thin section the carbonate is a distinctive dirty brown under plane-polarised light (PPL; Figure 5c), with high birefringence colours when viewed under crossed-polarised light (XPL; Figure 5d). On quartz vein contacts and along the margins of wall rock fragments where carbonate I is most abundant, the carbonate is characterised by sparry texture and individual crystals of up to 1.25 mm in length. Within the wall rock stage 2 carbonate veinlets and pressure fringes are comprised of a more massive and blocky form of carbonate I.

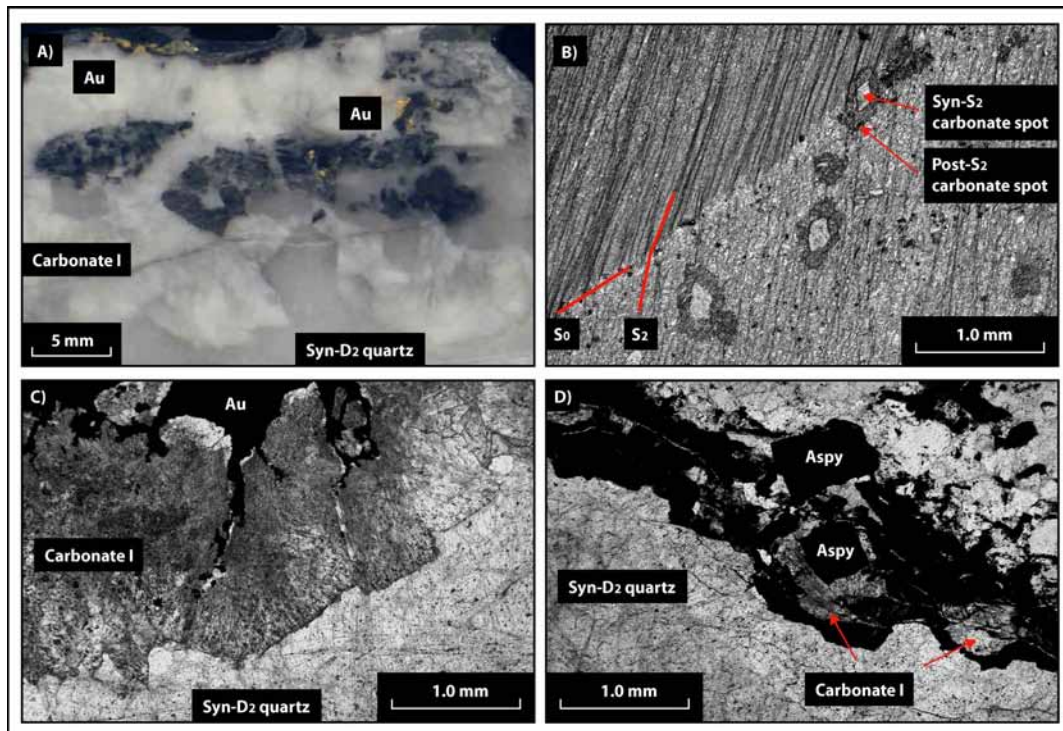


Figure 5. A. Carbonate I infill along a D_2 quartz vein margin. The carbonate I cements brecciated wall rock fragments and D_2 quartz. A slight alteration of the quartz from milky white to greyish-white is apparent. Minor gold occurrences are also visible. Sample S3SP1. Unorientated. Upper S3 saddle reef. B. Syn- S_2 carbonate spots encircled by post- S_2 carbonate I. PPL. Section dips at 90° towards 351° . Sample S3 111. C. Carbonate I infill along a D_2 quartz vein margin. Gold occurs as infill and replaces carbonate I. PPL. Unorientated thin section. Sample S3SP7. Upper S3 saddle reef. D. Carbonate I infill along a stylolitic seam. PPL. Unorientated thin section. Sample S3SP9.

Stage 3: Quartz I, carbonate II, sulphides II, muscovite, gold and carbonate III

Quartz I

Quartz I is present in minor amounts primarily as discontinuous 0.25-1 mm wide veinlets of fine-grained clear quartz, which are only evident in thin section (Figure 6a). Within the host sediments the quartz veinlets have two main forms, those with a rectangular or rhombic geometry that are associated with foliation boudinage, and those that constitute the entire internal portion of mm-scale D_3 kink bands (Figures 7a & 7b in Section B). Within D_2 quartz veins veinlets of quartz I occur proximal to vein contacts and may extend in to the wall rock for several millimetres. The veinlets crosscut and replace D_2 quartz and carbonate I (Figure 6a), and can be gold bearing. Quartz I can also be observed occurring as infill along reactivated D_2 vein contacts and in fractures within

stage 1 arsenopyrite. Within the host sediments quartz I pressure fringes occur on stage 1 sulphides and existing pressure fringes comprised mainly of carbonate I (Table 3).

The quartz within the fractured arsenopyrite is fibrous, as is the quartz that comprises the pressure fringes. The quartz that occurs as veinlets and as infill on reactivated D₂ vein margins has a more granular appearance.

Carbonate II

Carbonate II is a minor phase of mineral precipitation and like carbonate I, predominantly occurs as infill along reactivated D₂ quartz vein contacts (Figures 6b, c). Carbonate II is also present within D₂ quartz veins, where it occurs in association with stylolites and late fracture networks. Carbonate II also occurs on fractures and other lines of permeability within the host rock, but only in close proximity to D₂ vein margins. It is common for carbonate II in these settings to be accompanied by gold, although in numerous instances gold appears to post-date the carbonate. Carbonate II appears to have co-precipitated with quartz I and in some instances sulphides II, muscovite and gold (Table 3).

In hand specimen it is not possible to distinguish carbonate II, however, in thin section carbonate II is very distinctive. The carbonate is granular to equigranular (Figures 6b, c). Individual crystals are typically less than 0.2 mm in diameter and are often inclusion free. Under PPL carbonate II appears clear and colourless (Figure 6b), whilst under XPL the carbonate is predominantly pale brown with high birefringence (Figure 6c).

Sulphides II

Stage 3 sulphides consist of sphalerite, often with chalcopyrite inclusions (Figure 6d), chalcopyrite, galena and occasional pyrrhotite. Occurrences of these sulphides within D₂ quartz veins are minor, sporadic and restricted to infill along stylolites and late fractures. The more significant occurrences of stage 3 sulphides are associated with veinlets comprised of sulphides I ± carbonate I ± quartz I ± carbonate II, which occur within the wall rock up to several centimetres from the vein contact. Within these veinlets the stage 3 sulphides occur as infill predominantly along fractures in arsenopyrite and carbonate (sulphides I and carbonate I), and along quartz and/or carbonate grain boundaries (quartz I and carbonate II).

Individual sulphide grains rarely exceed 1mm in diameter, but their morphology is varied and strongly influenced by fracture patterns, existing mineral phases and co-precipitated mineral phases. The stage 3 sulphides post-date sulphides I and carbonate I, are syn- to post-quartz I and carbonate II, and pre- to syn-muscovite and gold (Table 3).

Muscovite

In hand specimen stage III muscovite is inconspicuous. In thin section occurrences of muscovite are relatively minor; however, this late-stage mineral is ubiquitous. The muscovite predominantly occurs as infill along reactivated margins of D₂ quartz veins (Figures 6b, c, e), along stylolites and late fractures, and within occurrences of carbonate II (Figure 6c). Muscovite also occurs as veinlets within the host sediments and as pressure fringes on stage 1 sulphides (Table 3).

Muscovite infill along D₂ vein contacts forms continuous bands up to 250 µm thick. Where the muscovite is in contact with carbonate I there is a clear alteration of the carbonate from dirty brown to pale white (Figure 6e). Muscovite commonly occurs in conjunction with carbonate II along D₂ vein contacts, where it may be either syn- or post-carbonate II. Occurrences of muscovite on stylolites and late fractures within D₂ quartz are negligible, whereas muscovite is abundant on fractures or other lines of permeability within the wall rock proximal to D₂ quartz vein contacts. Veinlets of muscovite within the host rock occur as an echelon sets of discontinuous lenticular veinlets and thin planar veinlets, both of which are related to mm-scale D₃ kink bands (see Figure 7c & 7d in Section B). It is not uncommon for a slight discolouration of the wall rock to be associated with the occurrence of muscovite. Pressure fringes comprised of muscovite clearly post-date the pressure fringes that consist of carbonate I and quartz I respectively. Small amounts of muscovite also occur within veinlets of carbonate I that have been deformed by mm-scale D₃ kink bands.

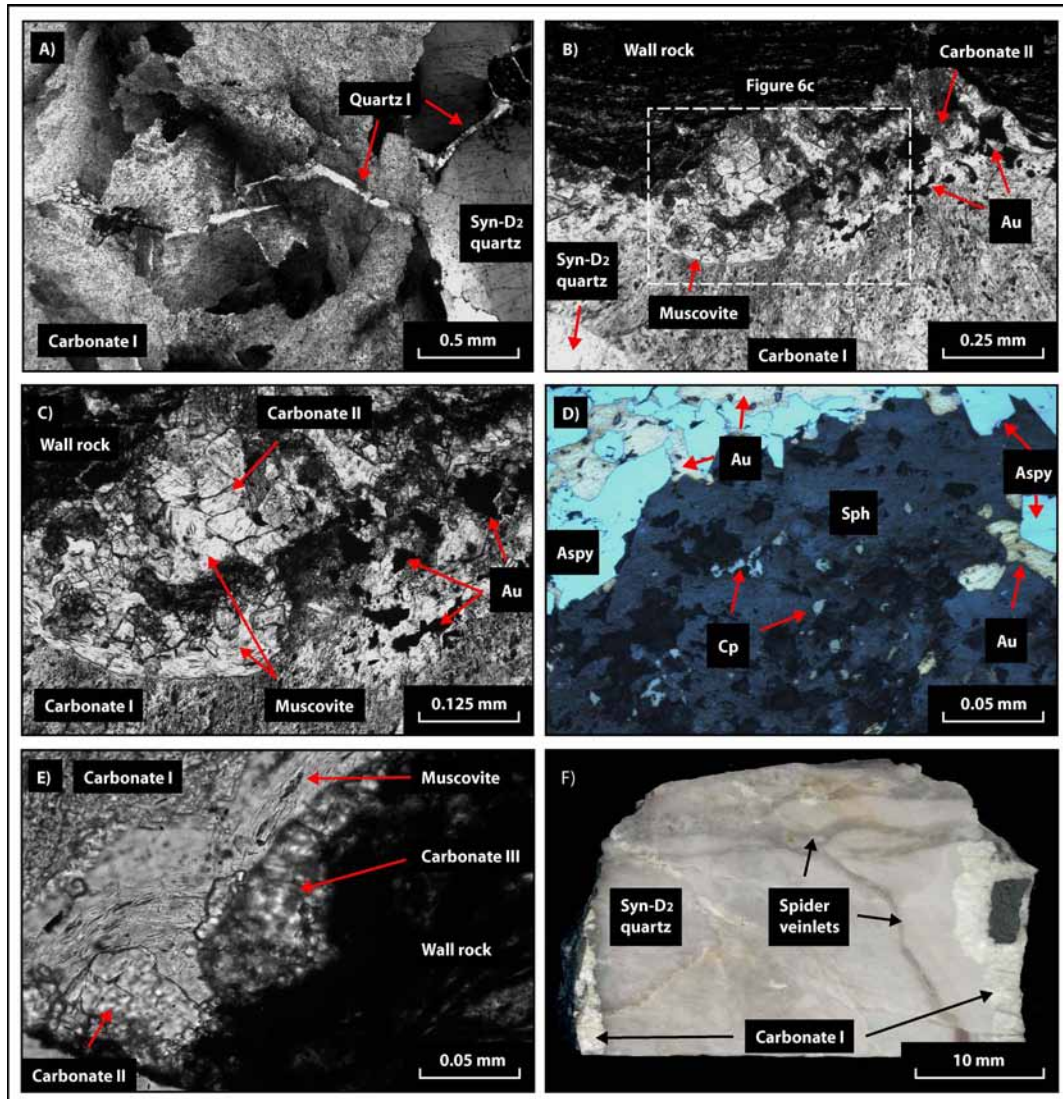


Figure 6. A. A minor veinlet of quartz I truncates carbonate I and D_2 quartz. XPL. Unorientated thin section. Sample S3SP7. Upper S3 saddle reef. B. Reactivated D_2 quartz vein contact. Infill consists of carbonate I followed by carbonate II, muscovite and gold. PPL. Unorientated thin section. Sample S3SP7. Upper S3 saddle reef. C. Enlargement from 6B. Granular carbonate II and muscovite infill are clearly visible. Alteration of carbonate I proximal to gold is evident in the right hand corner of the photomicrograph. XPL. Unorientated thin section. Sample S3SP7. Upper S3 saddle reef. D. Sphalerite (sph) with chalcopyrite (Cp) disease infilling fractured stage I arsenopyrite (Aspy). Gold post-dates the arsenopyrite, sphalerite and chalcopyrite. RL. Sample G11. Garrard's Reef. E. D_2 quartz vein contact with carbonate I, carbonate II and muscovite infill. There is minor alteration of carbonate I proximal to muscovite. Carbonate III overprints both carbonate II and muscovite. PPL. Unorientated thin section. Sample S3SP1. Upper S3 saddle reef. F. Section through a D_2 spur vein with carbonate I present on both vein margins. Spider veinlets crosscut the D_2 quartz and carbonate I, and are orthogonal to the vein margins. Unorientated sample. Sample G111. Garrard's Reef.

Gold

Individual gold particles observed during this study range in size from 5 μm up to 3500 μm (Figure 7). The majority of the gold occurs as infill along reactivated D_2 quartz vein contacts, particularly quartz-shale contacts (Figure 7a) and contacts that have been fractured and brecciated. The extent of the deformation associated with the reactivation of a D_2 vein contact is variable and may extend for several centimetres in to the quartz and/or wall rock.

Gold that occurs on reactivated D_2 vein contacts (Figures 7a, b) or within fractured or brecciated D_2 quartz proximal to vein contacts may be on its own as free gold or as infill within carbonate I, carbonate II or muscovite. Where gold is in contact with carbonate I there is a clear alteration of the carbonate from dirty brown to pale white (Figure 7b), and there are also far fewer inclusions within the altered zone, which may be up to 200 μm wide. Alteration of carbonate II and muscovite is also evident and occurs as a slight discolouration of the carbonate and muscovite where in contact with gold, however, alteration of carbonate II and muscovite is not always present. Gold also occurs in concurrence with quartz I, carbonate II and muscovite. The amount of mutually occurring quartz I, carbonate II, and muscovite associated with gold is solely dependent on the extent of dilation along the reactivated vein contact, but typically varies between single crystals and zones of infill up to 250 μm wide. Gold and muscovite can exhibit an intergranular relationship, whereby gold occurs as elongate prismatic grains bound by parallel fibrous crystals of muscovite. In such settings there is no alteration of the muscovite and the two minerals appear to have co-precipitated.

A significant amount of gold also occurs as infill along lines of permeability within the immediate wall rock, although such occurrences appear restricted to a zone that rarely extends for more than 10 mm from the vein margin (Figure 7b). These zones of deformed wall rock are intimately related to the reactivation of D_2 vein contacts. Within the wall rock gold can occur as free gold, as infill within stage I arsenopyrite, carbonate I, quartz I and carbonate II, or mutually with quartz I, carbonate II, sulphides II and muscovite. Where gold occurs in contact with carbonate I and carbonate II there is a clear alteration of the carbonate, as described above.

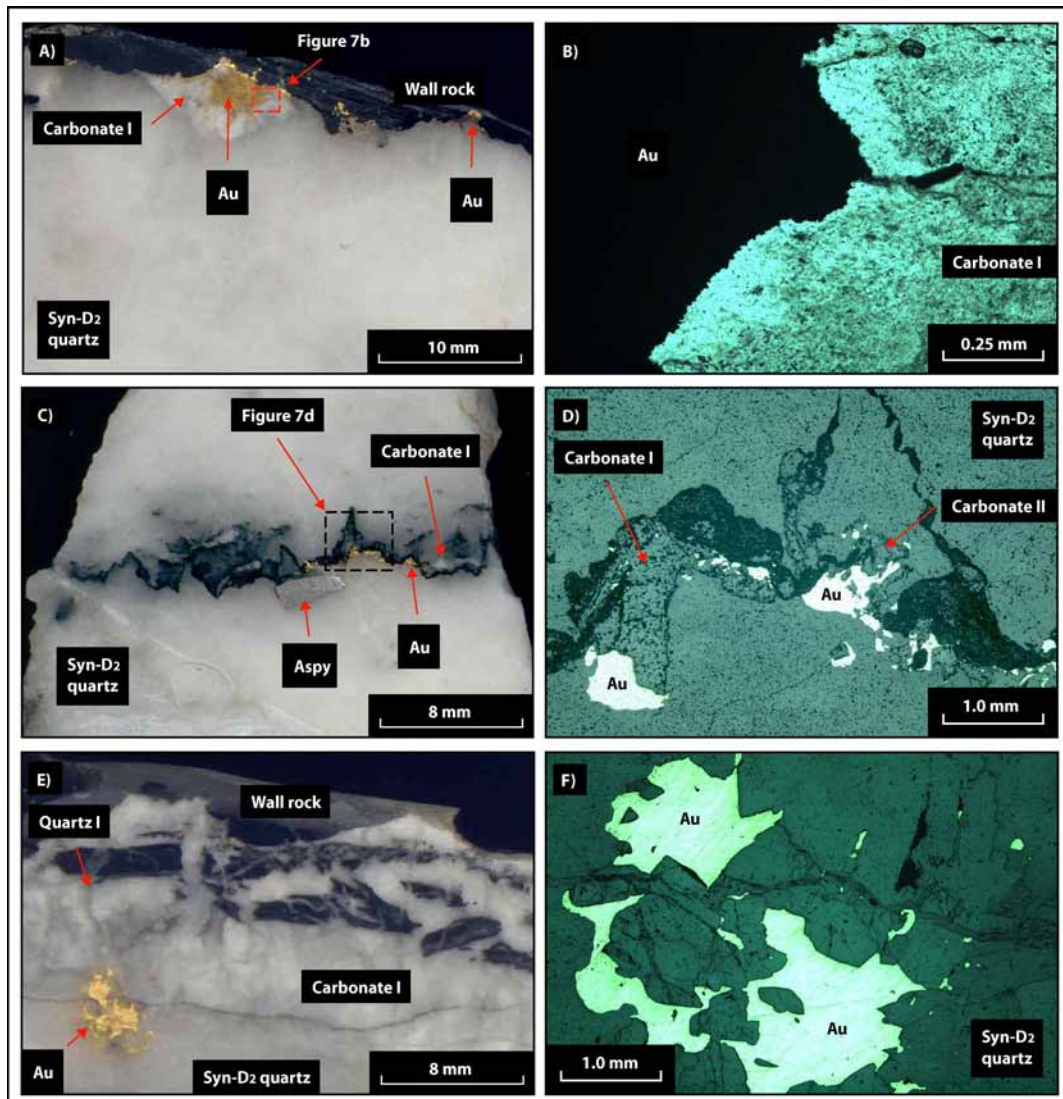


Figure 7. Gold occurrences. A. Gold occurring as infill within carbonate I and along a D_2 quartz vein contact. Unorientated sample. Sample S3SP7. Upper S3 saddle reef. B. Photomicrograph showing the alteration of carbonate I from dirty brown to pale white proximal to a gold grain. PPL. Unorientated thin section. Sample S3SP7. Upper S3 saddle reef. C. Stage 1 arsenopyrite (Aspy), carbonate I and gold occurring as infill along a stylolite. Sample S3SP9. Unorientated sample. Upper S3 saddle reef. D. Part of figure 7c in thin section. Gold post-dates carbonate I and appears concurrent with carbonate II. RL. Unorientated thin section. Sample S3SP9. Upper S3 saddle reef. E. Brecciated D_2 vein contact with fragments of wall rock and D_2 quartz cemented by carbonate I. Gold occurs as a coarse grain in D_2 quartz. Unorientated sample. Sample S3SP1. Upper S3 saddle reef. F. Photomicrograph showing part of the large gold occurrence shown in figure 7e. The occurrence of gold is clearly related to the crosscutting network of fractures, with no other late-stage mineral phases present. RL. Unorientated thin section. Sample S3SP1. Upper S3 saddle reef.

Coarse and irregularly distributed gold particles also occur as infill along stylolites (Figures 7c, d), which are orientated parallel to D₂ vein margins. However, in a number of instances where gold particles occur on stylolitic seams the gold is contained within cross cutting, orthogonal fractures. This also appears to be the case for some of the gold that occurs in association with wall rock laminae. Where gold occurs in association with stylolites it is often as infill within stage I arsenopyrite, and carbonate I. Where gold is in contact with carbonate I there is a clear alteration of the carbonate (as above). Gold also occurs with carbonate II, sulphides II and a minor amount of muscovite.

In hand specimen gold that appears as free gold within D₂ quartz (Figure 7e) is related to inconspicuous, but extensive fracture networks that are clearly visible in thin section (Figure 7f). The fracture networks display two general orientations; the dominant orientation is orthogonal to D₂ vein contacts, whilst the subordinate orientation is parallel to the vein margins. Gold associated with fractures tends to be coarse and sporadic, although generally the amount of fracture related gold increases proximal to reactivated vein contacts. Gold present on fractures predominately occurs as free gold or in association with quartz I, although occasionally the gold may occur with carbonate I and II, sulphides II and muscovite. It seems probable that auriferous quartz I veinlets are hosted by such fracture networks.

It is evident that gold post-dates sulphides I and carbonate I (Figures 8a, b), which in turn post-date the volumetrically significant phases of D₂ quartz (Figures 4c, d & Figure 5a). The relationships observed between gold, quartz I, carbonate II and sulphides II (Figures 8c, d) suggest that the deposition of gold occurred both during and after these three phases. The majority of gold-muscovite occurrences are indicative of co-precipitation (Figure 8e, f), however, in a number of localities gold replaces muscovite (Figure 8b; Table 3). No evidence to support more than one generation of gold was observed during this study.

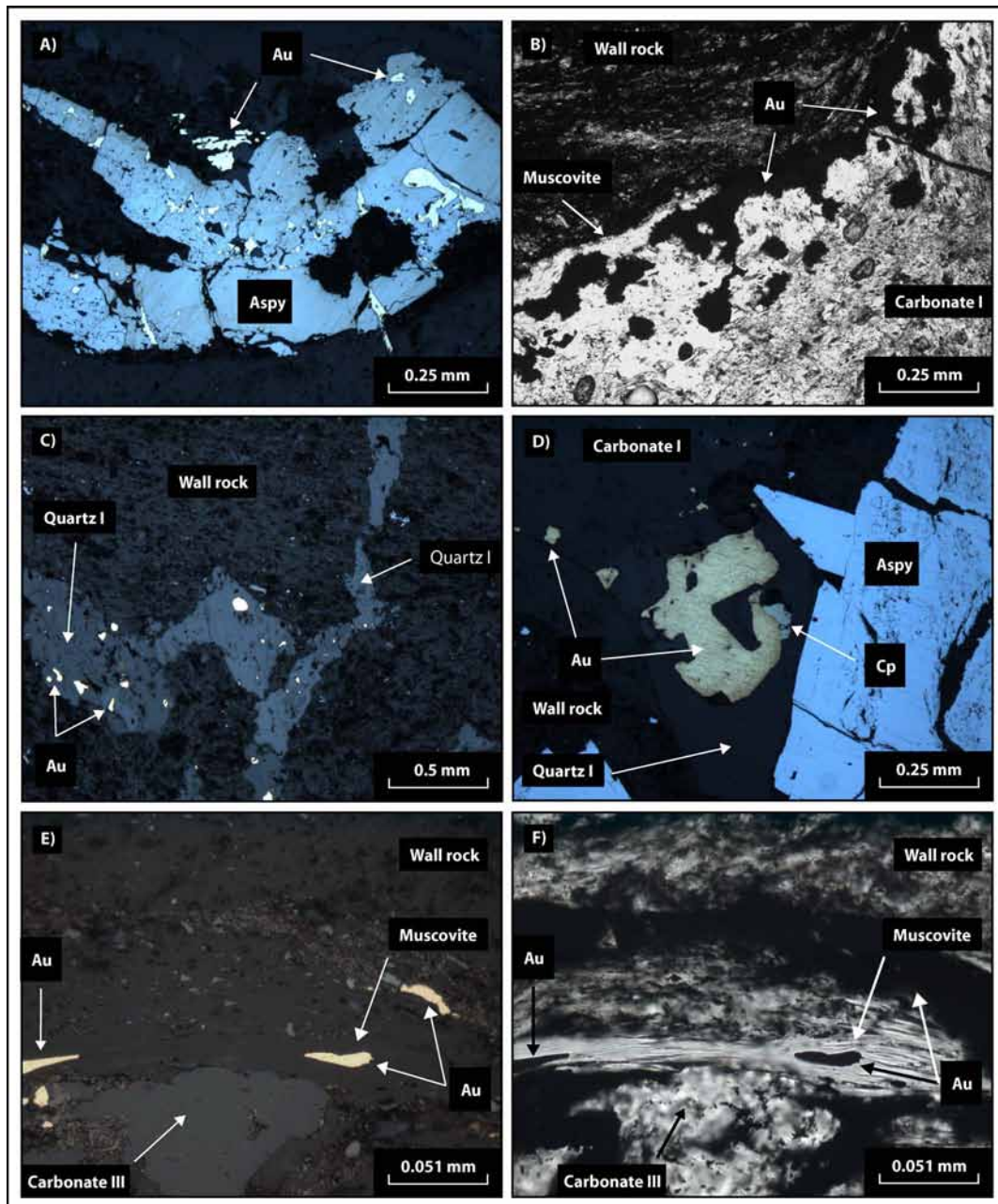


Figure 8. A. Gold in fractured stage I arsenopyrite (Aspy). RL. Unorientated thin section. Sample S3SP7. Upper S3 saddle reef. B. Reactivated D_2 quartz vein margin with carbonate I, muscovite and gold infill. An alteration of carbonate I and muscovite proximal to gold is evident. PPL. Unorientated thin section. Sample S3SP7. Upper S3 saddle reef. C. Gold within a veinlet of quartz I. RL. Unorientated thin section. Sample S3SP7. Upper S3 saddle reef. D. Gold and chalcopyrite within quartz I. RL. Unorientated thin section. Sample S3SP7. Upper S3 saddle reef. E & F. Gold, muscovite and carbonate III in wall rock proximal to a D_2 vein margin. Gold occurs concurrently with muscovite. Note the elongate gold grain within muscovite, right of centre. Carbonate III overprints muscovite. RL and PPL respectively. Unorientated thin section. Sample S3SP7. Upper S3 saddle reef.

Carbonate III

The occurrences of carbonate III is restricted to stylolites, late fractures and reactivated D₂ quartz vein contacts (Figures 6e & 8f). Carbonate III also occurs in association with minor fractures or lines of permeability within the host rock. Such discontinuities typically occur within a few centimetres of a D₂ vein margin and have commonly been exploited by numerous mineral phases (e.g. carbonate I and II). It is commonplace for the occurrence of carbonate III to be proximal to gold, although in a few instances it could be argued that gold and carbonate III were coeval.

Carbonate III can only be observed in thin section, where under PPL it appears as poorly defined, clear crystals of carbonate characterised by darkened and sometimes fuzzy margins (Figure 6e). Under XPL the carbonate is brown to dirty brown in colour and the poor crystal definition is made more apparent by an outward darkening of a crystals colour. It would appear that carbonate III is an alteration that overprints carbonate II and partially overprints muscovite in a number of localities. It is suggested that carbonate III is in fact an alteration of carbonate II, which resulted from the introduction and precipitation of gold (Table 3).

Stage 4: Quartz II

Quartz II is colourless, occurring as 1-5 mm wide comb spider veinlets and phantom spider veinlets (Figure 6f; Dowling & Morrison, 1989). Comb spider veinlets are characterised by vugs and euhedral quartz crystals orientated perpendicular to the vein margins, whereas phantom spider veinlets are comprised of interlocking anhedral quartz crystals and are devoid of vugs and inclusions. It is not uncommon for a small amount of white to off-white carbonate to be associated with comb spider veinlets. Both forms of spider veinlet are ubiquitous and generally orthogonal to D₂ vein margins; however, in a few instances veinlets occur parallel with D₂ vein margins. Spider veinlets clearly post-date stages 1 to 3 indicating that quartz II was the last phase of mineral precipitation within the auriferous vein systems (Table 3).

DISCUSSION

The late-stage paragenetic sequence (Table 3) consistently observed within auriferous quartz veins and within the host rock is indicative of an evolving system, both structurally and mineralogically. Stage 1 sulphides occur as infill within D₂ quartz veins and as a pervasive alteration of the wall rock (see Kwak & Li, 1996; Li *et al.*, 1998; Bierlein *et al.*, 1988; Figure 4b, c). A minor amount of stage 1 arsenopyrite and pyrite also occurs as infill along stylolites and fractures that crosscut D₂ quartz (Figure 4d). It is suggested that stage 1 sulphides represent the final phase of mineral growth associated with D₂ quartz veins and that the initial development of stylolites and fractures is associated with progressive, but weakening deformation during the latter part of D₂ (Table 3).

Stage 2 carbonate (carbonate I; Table 3) is the most abundant of the late-stage mineral phases and occurs predominantly along reactivated and brecciated D₂ quartz vein contacts (Figures 5a, 6f & 7a). Stage 2 carbonate clearly post-dates D₂ quartz veins and stage 1 sulphides, and is evidently related to a subsequent period of reactivation and brittle deformation. The relative timing of carbonate I is most apparent within the host rock where veinlets of carbonate I truncate S₂ but are deformed by S₃. Carbonate I represent a period of reactivation, brecciation, brittle fracturing and renewed pressure solution (Figure 7c) that may mark the beginning of D₃. Carbonate I could correspond to the occurrences of ankerite reported by Lindgren (1920) and Chace (1949).

The mineral phases associated with stages 3 (Figures 6, 7 & 8; Table 3) represent progressive episodes of mineral growth, which predominantly occur in the same structural settings and clearly post-date D₂ quartz, stage I sulphides and stage II carbonate. The structural settings include reactivated and often brecciated D₂ vein contacts, fracture networks and stylolites. Within the host rock quartz I and muscovite occur as pressure fringes on stage 1 sulphides and as veinlets that are related to the formation of D₃ extensional kink bands (Section B).

The stage 4 spider veinlets (Figure 6f) are similar in orientation to the fracture networks that host stage 2 and 3 mineral phases. This suggests that the spider veinlets formed within a similar, if not the same strain field. Spider veinlets have also been reported by Stone (1937), Chace (1949), Stillwell (1953), Thomas (1953b) and Jia *et al.*, (2000).

The spider veinlets represent a late episode of brittle fracturing that occurred late in D₃ (Table 3).

The occurrence of gold within the Bendigo Goldfield

This study has observed gold in each of the settings reported by Chace (1949), Thomas (1953b), Wilkinson (1988b), Forde (1989), Sharpe & MacGeehan (1990), Jia *et al.* (2000) and Johansen (2001b), with the exception of spider veinlets. Differences between barren and auriferous quartz veins, other than the occurrence of visible gold, are often inconspicuous to the naked eye, which is consistent with the observations of Stillwell (1950). Such differences relate to the subsequent deformation of the quartz veins and the occurrence of discrete, late mineral phases (e.g. Figures 6 & 7).

This study has shown that gold occurrences at Bendigo are associated with three structural and micro-structural settings:

1. Reactivated D₂ quartz vein contacts (Figures 7a, b);
2. Stylolites in D₂ quartz (Figures 7c, d); and
3. Fractures and fracture networks in D₂ quartz (Figures 7e, f).

It is proposed that the reactivation of D₂ vein contacts and the deformation of quartz and wall rock proximal to a contact (Figure 9) were simultaneous with the development of fractures. This is supported by an increase in the frequency of fractures and the amount of fracture-related gold proximal to reactivated D₂ vein contacts. Gold-bearing stylolites are orientated parallel to sub-parallel with the vein margins, which is indicative of ~ENE-WSW shortening during D₂ and D₃. The amplification of stylolites during D₃ may have reached a critical point whereby the process of pressure solution enabled the transport of solution by diffusive mass transfer (Blenkinsop, 2000). However, in the majority of instances it is only the stylolites that are proximal to a D₂ vein margin that are gold bearing. This suggests that a degree of connectivity between a vein contact and stylolite during reactivation was essential in order for auriferous fluids to access the stylolite. In some instances where a significant amount of gold occurs on a stylolite, the occurrence of gold is related to crosscutting fractures. In such cases the fractures may have allowed auriferous fluid to access the stylolite where the carbonaceous residue may have acted as a loci for gold precipitation (c.f. Bierlein *et al.*, 2001a).

In terms of mineral paragenesis, gold occurs as infill within stage I arsenopyrite, carbonate I, carbonate II and occasional muscovite, all of which post date the volumetrically significant phases of D₂ quartz. Gold is synchronous with quartz I, carbonate II, sulphides II and muscovite. Only one generation of gold was observed during this study, however, it must be emphasised that only economic occurrences of gold were investigated.

The relative timing of gold within the Bendigo Goldfield

The relative timing of gold has been established on the basis of structural setting and associated mineral phases. Gold is restricted to a single stage mineralising event (stage 3; Table 3) and occurs in association with reactivated D₂ quartz vein contacts, fractures and stylolites, all of which post date D₂ quartz veins associated with D₂ folds and faults (Figure 7; c.f. Stillwell, 1922, 1950; Jia *et al.*, 2000; Schaubs & Wilson, 2002). The revised late-stage mineral paragenesis demonstrates that gold was in part, synchronous with quartz I, carbonate II, sulphides II, muscovite and carbonate III (Table 3). This is in partial agreement with Stone (1937) and Chace (1949), who states, “it may be considered that inter-mineralisation fracturing and brecciation, and deposition of late quartz, sulphides and gold, were superimposed on the quartz bodies” (p. 597).

The reactivation, brecciation and brittle fracturing of the deposit may have been episodic and in response to D₃ kinking. A link between the development of D₃ extensional kink bands and veinlets comprised of quartz I and muscovite has been established in Section B. Strain partitioning during D₃, whether in the form of kilometric-scale kinks (Section B), zones of intense S₃ (Figure 9) or single mm-scale kink bands (Section B), was apparently fundamental in developing and maintaining zones of permeability. It is therefore proposed that gold deposition occurred during D₃, and more specifically, in association with the development of D₃ kink bands (e.g. Figure 9).

The revised late-stage paragenesis represents a logical and progressive sequence of events, which integrate D₂ and D₃ in a manner that is indicative of a single orogenic event. It is therefore proposed that D₃ and the timing of gold deposition correspond to the later stages of the Benambran Orogeny (see VandenBerg *et al.*, 2000; Sections A & B).



Figure 9. Photograph showing the eastern margin of the D3 leg reef shown in Figure 3f. Two sets of well-developed L_2^3 intersection lineations, one set pitching north (A) and one set south (B), are clearly visible on the hangingwall. Visible gold occurrences, marked by pink circles, only occur where D₂ quartz has been reactivated proximal to the vein margin. The occurrence of L_2^3 intersection lineations defines a zone of high strain, which corresponds to the occurrence of gold. D3 Leg reef, Deborah Anticline. View to the northeast.

Geochronological research (Arne *et al.*, 1998, 2001; Foster *et al.*, 1998; Bierlein *et al.*, 2001b, c, d) constrains the formation of most major gold deposits within the Stawell and Bendigo Zones, which includes the Bendigo Goldfield, to a broad interval of time spanning the Late Ordovician to Silurian (*ca.* 455-435 Ma; D₂-D₃? Section A).

At Bendigo, Foster *et al.* (1998) dated sericite from an auriferous quartz vein exposed in the Central Deborah Mine. A mean age of ~440 Ma was determined from ⁴⁰Ar-³⁹Ar data and taken to represent the time of sericite crystallisation and vein formation. Bierlein *et al.* (2001c) reported additional ⁴⁰Ar-³⁹Ar geochronological data, which significantly expanded upon, yet supported the initial findings of Foster *et al.* (1998). Re-Os dating of sulphides closely associated with the gold mineralisation at Bendigo utilised samples of arsenopyrite and pyrite (Arne *et al.*, 2001). The arsenopyrite analyses yielded a mean model age of 446 ± 5 Ma, whereas a five-point isochron based on three pyrite analyses,

in addition to the arsenopyrite analyses, yielded an age of 438 ± 6 Ma, a figure comparable to the ^{40}Ar - ^{39}Ar data presented in Foster *et al.* (1998) and Bierlein *et al.* (2001c).

However, this study only recognises one generation of sericite, the occurrence of which is synchronous with the formation of D₂ quartz veins but more importantly pre-dates the economic occurrences of gold (D₃; Table 3). Likewise, arsenopyrite and pyrite (Stage I sulphides; Table 3) also pre-date the economic occurrences of gold at Bendigo (D₃).

Based on the structural chronology presented in Sections A & B and the new paragenesis for late-stage mineralisation presented in this contribution, it is proposed that the relative timing of economic gold occurrences (D₃) corresponds to the later stages of the Benambran Orogeny (*ca.* 439-435 Ma). It is also proposed that D₂ and D₃ represent a logical and progressive sequence of events indicative of a single orogenic event (Benambran Orogeny). In light of these findings it is suggested that the geochronological age constraints on the timing of gold deposition at Bendigo, as obtained from ^{40}Ar - ^{39}Ar and Re-Os isotope data (Foster *et al.*, 1998; Arne *et al.*, 2001; Bierlein *et al.*, 2001c), either define a maximum age for economic gold occurrences or the timing of an earlier, economically subordinate phase of gold deposition, which this study did not observe.

In order to quantify the timing of D₃ with respect to the models of Vandenberg *et al.* (2000) and more accurately constrain the timing of economic gold occurrences at Bendigo, specific age dating of D₃ mineral assemblages (e.g. muscovite and stage 3 sulphides) is required.

CONCLUSIONS

1. A consistent four-stage mineral paragenesis, which includes gold, post-dates the quartz veins associated with D₂ folding and faulting.
2. Structurally, gold is primarily associated with reactivated D₂ quartz vein contacts, fractures and stylolites, all of which relate to deformation during D₃.
3. Mineralogically, gold was co-precipitated with syn-D₃ mineral assemblages, including quartz I, carbonate II, sulphides II, muscovite and carbonate III.

4. In agreement with Stone (1937); Chace (1949); Thomas (1953b) and Wilkinson (1988b) galena, chalcopyrite and sphalerite (sulphides II) maybe regarded as good proxies for gold.
5. It is proposed that deformation relating to D₂ and D₃ was progressive and that D₃ represents the later stages of the Benambran Orogeny (*ca.* 439-435 Ma).
6. It is suggested that current geochronological constraints on the timing of gold at Bendigo may define a maximum age for economic gold occurrences or the timing of an earlier, economically subordinate generation of gold that was not observed by this study.
7. A revised relative timing of gold combined with a revised structural chronology has significant implications for the economic exploitation of the Bendigo Goldfield.

SECTION D

STRUCTURAL CONTROLS ON THE LOCATION OF ORE SHOOTS WITHIN THE BENDIGO GOLDFIELD, CENTRAL VICTORIA, AUSTRALIA: IMPLICATIONS FOR NEAR MINE EXPLORATION

Abstract

Within the Bendigo Goldfield the ability to predict ore shoot location and orientation is critical to exploration particularly given that the structural framework is complex and involves five-stages of deformation (D_1 - D_5). It has recently been established that auriferous mineralisation post-dates the peak of deformation and metamorphism (D_2) and was synchronous with the development of D_3 kink bands. Spatial analysis of historical production data has revealed five previously unrecognised high-grade trends. These trends do not correspond to the orientation of D_3 kink bands, but instead coincide with the intersection axis between a kink band axial plane and bedding or bedding parallel structure. It is proposed that the intersection axes control ore shoot geometry and location because they also correspond to the orientation of historically worked ore shoots and those encountered more recently by Bendigo Mining Ltd. A new understanding of the controls on ore shoots has considerable implications for future exploration within the goldfield and elsewhere in central Victoria.

Key words: Bendigo Goldfield, auriferous mineralisation, ore shoots, exploration.

INTRODUCTION

A number of early workers in the Bendigo Goldfield have acknowledged a poor understanding of the controls on gold localisation and ore shoot formation (e.g. Dunn, 1896; Whitelaw, 1914; Chace, 1949; Thomas, 1953b). Whereas Wilkinson (1988b), Sharpe & MacGeehan (1990), Johansen (2001b), Johansen *et al.* (2003) and Dominy & Johansen (2004) are of the opinion that the quartz veins are simply characterised by an erratic gold distribution, with little or no reference made to the possibility of deficient geological understanding. A revision of the deformation chronology (Sections A & B) and relative timing of gold (Section C) has indicated that the structural evolution of the goldfield is more complex than previously thought and that economic gold occurrences are associated with a deformation event that was previously unrecognised. These findings have significant implications for identifying and resolving the controls on ore shoot formation, location and geometry.

The aim of this contribution is to investigate high-grade trends within the Bendigo Goldfield in an attempt to resolve their underlying structural control(s). A summary of the regional and local geology is presented together with a review of previous ideas on ore shoot formation and location. The implications for future exploration are discussed.

REGIONAL GEOLOGY

The Bendigo Goldfield is located within the Western Subprovince (WSP; Gray *et al.*, 1997) of the Lachlan Fold Belt (LFB; Glen, 1992; Gray & Foster, 1998, 2004; Foster & Gray, 2000; Bierlein *et al.*, 2002; Gray *et al.*, 2002), which, itself, is part of the Palaeozoic Tasman Fold Belt of eastern Australia (Figure 1a; Ramsay & VandenBerg, 1986; VandenBerg *et al.*, 2000). The geology of the WSP comprises three fault-defined structural zones (Stawell, Bendigo and Melbourne; Figure 1a, b; Gray, 2003) that are dominated by deformed and metamorphosed Cambro-Ordovician to Silurian turbidites (Cas & VandenBerg, 1988; Gray & Foster, 2000; VandenBerg *et al.*, 2000; Fergusson, 2003). The metasediments typify medium-*P/T* (Barrovian type) conditions and predominantly exhibit sub-greenschist to greenschist facies metamorphism (Cox *et al.*, 1991a; Offler *et al.*, 1998).

Deformation within the WSP is characterised by a mostly east-vergent, N-S to NW-SE striking, fold and thrust belt, the formation of which has been attributed to a thin-skinned style of crustal shortening (Gray & Willman, 1991a, b, c; Cox *et al.*, 1991b; Foster & Gray, 2000; Gray & Foster, 2000, 2004). Geochronological research (Arne *et al.*, 1998; Foster *et al.*, 1998; Bierlein *et al.*, 2001b, c) has demonstrated that metamorphism and deformation was diachronous and that the fold and thrust belt formed in response to episodic, eastward-progressing deformation during the Late Ordovician to Middle Devonian (*ca.* 455-385 Ma).

Emplacement of dyke swarms and felsic to intermediate intrusions with S- and I-type affinities occurred within the WSP over two broad intervals. The first, between ~415-395 Ma (Late Silurian to Early Devonian), was primarily restricted to the Stawell Zone and south-western, western and north-central parts of the Bendigo Zone, whereas the second, which occurred between ~385-365 Ma (Middle to Late Devonian), affected the Melbourne Zone, most of the Bendigo Zone and the eastern part of the Stawell Zone (Richards & Singleton, 1981; Foster *et al.*, 1998; Bierlein *et al.*, 2001b, c, d). A younger period of lamprophyre dyke emplacement has been dated at 155 Ma (Jurassic) by McDougall & Wellman (1976).

THE IMAGES ON THIS PAGE HAVE BEEN REMOVED DUE TO
COPYRIGHT RESTRICTIONS

Figure 1. *A. The Lachlan Fold Belt (LFB) of mainland Australia. Adapted from Gray et al. (1997). B. The location of Bendigo within the Bendigo Zone (BZ). Adapted from Gray and Willman (1991a). C. Geological map of the Bendigo region, showing biostratigraphic units, intra-zone faults and the Bendigo Goldfield. Adapted from Johansen (2001b).*

LOCAL GEOLOGY

Within the WSP the Bendigo Goldfield is located within the Bendigo Zone (BZ; Gray, 2003) approximately 5 km northeast of the Harcourt granodiorite (Figure 1b). The goldfield is hosted by a NNW zone of deformed, Lower to Middle Ordovician metasediments bound by the intrazone Whitelaw thrust fault to the east and the Sebastian thrust fault to the west (Figure 1c). The metasediments, which are characteristic of the Bendigo Zone, correspond to part of the Castlemaine Supergroup (Figure 1c; Cas & VandenBerg, 1988; Willman & Wilkinson, 1992) and comprise sandstones, siltstones, shales, thin polymict conglomerates and occasional cone-in-cone limestones (Cas, 1983; Cas & VandenBerg, 1988; Sharpe & MacGeehan, 1990; Willman & Wilkinson, 1992). The metasediments, which are predominantly turbidites, often exhibit the sedimentary characteristics of Bouma cycles, suggesting that sedimentation took place in a deep-sea submarine fan environment (Cas, 1983; Cas & VandenBerg, 1988; Sharpe & MacGeehan, 1990; Turnbull & McDermott, 1998).

Deformation history

The construction of a new underground mine within the Bendigo Goldfield presented a unique opportunity to reinvestigate the structural history (Forde, 1989; Schaub & Wilson, 2002). Section A reports several tectonic foliations, both proximal and distal to auriferous mineralisation. The presence of multiple foliations, which in numerous instances post-date the prominent axial planar cleavage (S_2), suggests that the deformation history is more complex than previously thought. Based primarily on the recognition of overprinting tectonic foliations (S_1 - S_5), a revised five-stage deformation history (D_1 - D_5) has been proposed for the Bendigo Goldfield (Sections A & B; Figure 2).

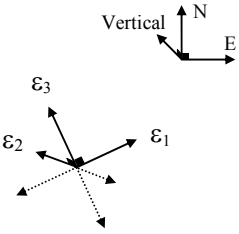
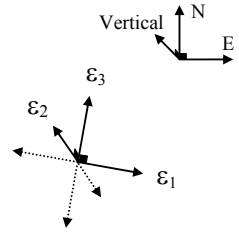
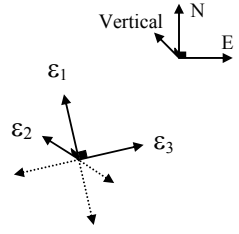
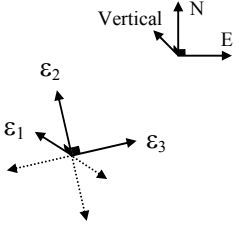
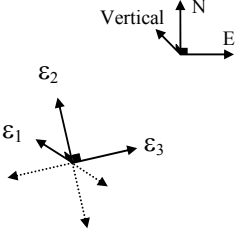
Proposed Orogenic Timing	Deformation Stage	Principal Extension Directions ($\epsilon_1 > \epsilon_2 > \epsilon_3$)	Key Attributes
Kamiblan Orogeny (ca. 360-340 Ma)	D ₅		<ul style="list-style-type: none"> • Millimetre-scale (S₅) dextral contractional kink bands • No associated mineral phases
Tabberabberan Orogeny (ca. 381-377 Ma)	D ₄		<ul style="list-style-type: none"> • Millimetre-scale (S₄) to metre-scale (F₄) sinistral contractional kink bands • No associated mineral phases
Benambran Orogeny (ca. 439-435 Ma)	D ₃		<ul style="list-style-type: none"> • Late-stage mineral phases, including gold • Millimetre-scale (S₃) to kilometre-scale (F₃) extensional kink bands • Oblique faults
	D ₂		<ul style="list-style-type: none"> • Major quartz veins (e.g. saddle reefs) • Deposit scale reverse faults • Axial planar crenulation cleavage (S₂) • Mesoscopic chevron folds (F₂)
	D ₁		<ul style="list-style-type: none"> • Pre-F₂, bedding parallel laminated quartz veins • Sub-horizontal tectonic foliation (S₁) • Inter- & intra-zone thrust faults

Figure 2. Summary of the five-stage deformation history proposed for the Bendigo Goldfield (Sections A, B & C). ϵ_1 , ϵ_2 and ϵ_3 define the principal strain axes within the strain ellipsoid.

Deposit scale controls on gold localisation

At Bendigo, gold is primarily associated with quartz veins (e.g. Dunn, 1896; Stillwell, 1922; Chace, 1949; Thomas, 1953b; Wilkinson, 1988b; Sharpe & MacGeehan, 1990; Cox *et al.*, 1991a; Willman & Wilkinson, 1992; Jia *et al.*, 2000; Schaub & Wilson, 2002; Section C), the geometry of which relates intimately to the structural evolution of the goldfield (Figure 2; Forde, 1991; Schaub and Wilson, 2002; Sections A & B). Within the quartz veins occurrences of gold are renowned for their erratic distribution, a characteristic that appears to be independent of scale (Dunn, 1896; Whitelaw, 1914; Chace 1949; Thomas, 1953b; Wilkinson 1988b; Sharpe & MacGeehan, 1990; Johansen, 2001; Johansen *et al.*, 2003; Dominy & Johansen, 2004). In spite of this a number of high-grade shoots were profitably worked for in excess of a kilometre (e.g. Stillwell, 1922, p. 10. and Thomas, 1953b, p. 1026), although Thomas (1953b) emphasised that the shoots may have contained barren zones, albeit of insufficient length to prevent stopping.

Previous ideas

Despite the apparent continuity of some high-grade shoots (e.g. Stillwell, 1922) a number of early workers have acknowledged a poor understanding of the controls on gold localisation and ore shoot formation (e.g. Dunn, 1896; Whitelaw, 1914; Chace, 1949; Thomas, 1953b). Thomas (1953b) stated, “no obvious structural control of the location of payable shoots has been discovered”, whereas Chace (1949) was of the opinion that the origin, localisation and position of high-grade shoots could probably be resolved by investigating late fracturing, brecciation, vein re-opening and late mineralisation (Section C).

It was recognised during the early development of the goldfield that auriferous reefs and D₂ faults occurred at regular vertical intervals, with little or no mineralisation in-between. Dunn (1896) proposed that there were “certain horizons more favourable to the presence of gold”; however, Herman (1923) demonstrated that ore shoots occurred throughout most of the sedimentary succession. Stone (1937) favoured a structural rather than a stratigraphic explanation for the apparent relationship between lithology and vein type, stating, “the connection between faults and payable reefs is amply proved” and that faults “may be connected with different, but as yet unrecognised, lithologic facies of the Ordovician section”. Historical research undertaken by Bendigo

Mining Ltd., combined with diamond drilling and a three-dimensional reconstruction of historical workings provided additional data supporting the theory that reefs or clusters of reefs, termed 'ribbons', occurred at regular vertical intervals. This theory has since been developed into the 'ribbon repeat model' (Johansen, 2001b) and clearly represents an important control on the localisation of gold within the field.

Whitelaw (1914) reported that a "steep pitch appears favourable for gold location, and N-pitching portions of the reefs appear to be richer than S-pitching portions". "A statistical study of the field has brought out a close spatial relationship between gold-bearing quartz reefs and gentle domes along the anticlines" (Bendigo Mines Ltd., 1935, as reported in Stone, 1937). Stone (1937) stated, "payable gold production and major faulting are definitely related to the main domes and the northern slopes of those domes". Chace (1949) agreed, "the more productive ore bodies have been found along the anticlines in the area of the domes, particularly where the plunge is to the north", although Thomas (1953b) only went as far as acknowledging a "general association of the more productive mines with domal structures". It is suggested by Cox *et al.* (1991a) that the culmination zones controlled regional fluid migration patterns and fluid pressure regimes, with a "progressive upwards migration of fluids along high permeability beds and bedding-concordant fault zones, not just towards anticlinal hinge zones, but also up plunging fold hinges towards the anticlinal culmination zones".

Forde (1989), who proposed a late orogenic timing for gold, suggested that the location and orientation of high-grade shoots was controlled by the intersection of D₄ high strain zones with favourably orientated D₂ structures. In the KK mine on the Hustler's line of reef ore shoots in the east leg pitched northwards at 15°-30° (Whitelaw, 1914). Forde (1989) stated, "this orientation is coincident with the intersection of the east leg with S₄ and can be explained by gaping and brecciation during D₄".

This review shows that within the goldfield (Figure 1c) auriferous mineralisation occurs at regular vertical intervals, particularly on north and south plunging F₂ folds proximal to domal culminations (Whitelaw, 1914, Chace, 1949; Thomas, 1953b; Forde, 1989; Cox *et al.*, 1991a). There is disagreement regarding the cause of F₂ plunge reversals and the relative timing of gold mineralisation with respect to the plunge reversals (e.g. Whitelaw, 1914; Stone, 1937). In the case of the latter, a dichotomy exists between views that auriferous mineralisation was synchronous with the formation of domal culminations (e.g. Whitelaw, 1914; Stone, 1937), and views that the mineralisation post

dated the formation of domal culminations (e.g. Forde, 1989). This difference of opinion relates primarily to the structural evolution of the goldfield, which itself has been a matter of contention (see Sections A, B & C). The resolution of this disagreement is of fundamental importance to the future exploitation of the goldfield.

Recent developments

A reinvestigation of the structural chronology preserved within the Bendigo Goldfield has recognised kilometre-scale kink bands (F_3 ; Figure 3a; Sections A & B). The orientation and geometry of F_3 corresponds to the alignment of domal culminations across the goldfield (Figures 3b, c & 4a, b; Sections A & B) and therefore the high-grade gold occurrences reported by Whitelaw (1914); Stone (1937); Chace (1949) and Thomas (1953b). Section C demonstrates that local-scale gold occurrences are restricted to three structural and micro-structural settings, all of which post date the D_2 quartz veins and are believed synchronous with the formation of D_3 kink bands (Figure 2). At a goldfield-scale there is also an apparent spatial relationship between the more productive areas of the goldfield and the location of F_3 axial traces (Figure 3c). It has been proposed that during D_3 , zones of higher strain, whether in the form of F_3 kink bands or zones of intense S_3 , were fundamental in developing and maintaining permeability during mineralisation (Section C).

THE IMAGES ON THIS PAGE HAVE BEEN REMOVED DUE TO
COPYRIGHT RESTRICTIONS

Figure 3. A. F_2 axial traces within the limits of the goldfield. The location of F_3 is shown in grey and superimposed on part B & C. Modified from Section A. B. The location of domes along F_2 anticlines and the most productive sections of the anticlines as defined by Stone (1937). Modified from Stone (1937). C. The location of the most productive portions of the F_2 anticlines as defined by Thomas (1953b). Modified from Thomas (1953b).

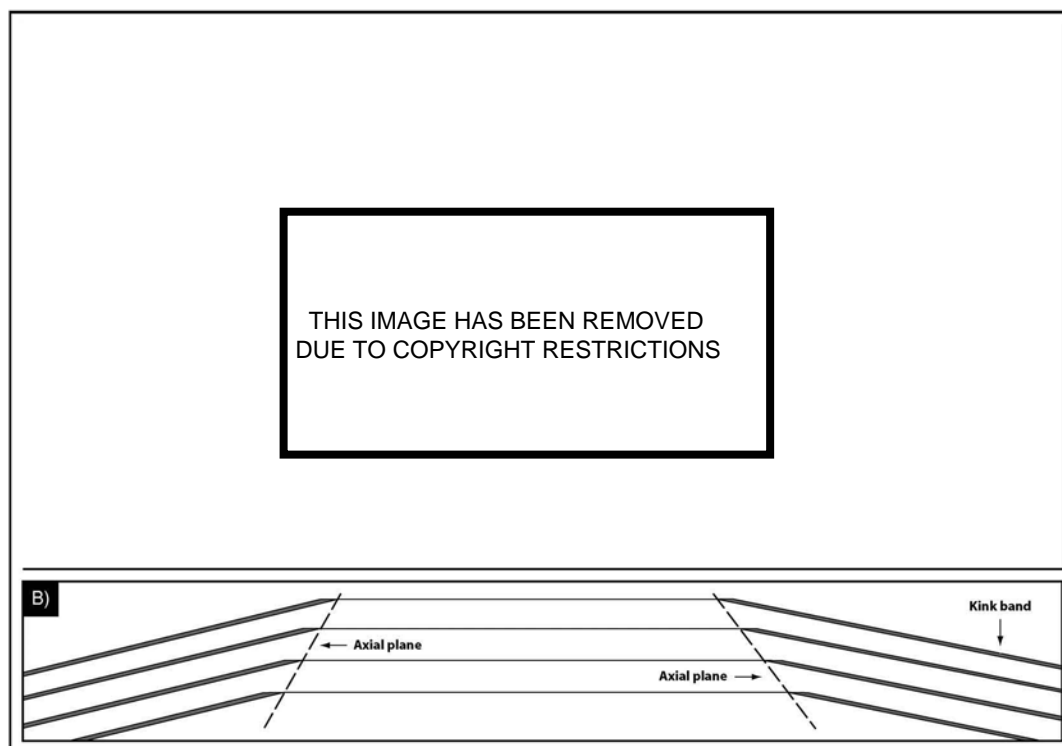


Figure 4. A. Vertical longitudinal section of part of the New Chum Anticline. Historical workings are more extensive on the south and the north plunging sections. Modified from Johansen, (2001b). B. Idealised cross-section through conjugate kink bands with extensional geometry. The geometry of the kink bands is comparable to the stoping outline shown in A.

SPATIAL ANALYSIS OF HISTORICAL PRODUCTION

Fry analysis

The purpose of Fry analysis (Fry, 1979) is to reveal or enhance patterns of spatial distribution. The technique of Fry analysis was originally derived from strain analysis in structural geology (Fry, 1979; Hanna & Fry, 1979) and has since proved an effective means of modelling the spatial distribution of mineralisation (Vearncombe & Vearncombe, 1999; Blenkinsop, 2002; Kadzviti, 2003; Kreuzer, 2003).

By applying Fry analysis to mineral deposits Vearncombe & Vearncombe (1999) demonstrated that “at the regional scale, Fry analysis can assess distribution patterns of mineralisation and potential controlling structures” and that “at the deposit scale, the characteristics of zones of mineralisation such as direction, spacing, high-grade ore direction, and grade distribution can all be deduced”. A combination of Fry analysis and geological understanding is therefore a powerful means of investigating the distribution

of, and the controls on, mineralisation, which in turn has significant implication for both near mine and regional exploration (e.g. Kadzviti, 2003; Kreuzer, 2003).

Although the technique of Fry Analysis (Fry, 1979) can operate manually it is laborious and therefore best applied through the use of computer programs (e.g. Vearncombe & Vearncombe, 1999; Blenkinsop, 2002; Kreuzer, 2003; Wormald *et al.*, 2003). The technique utilises data comprised of point localities for features such as ore deposits or mine shafts (e.g. Figure 5a). The spatial relationship between one point and the other points in a dataset may be defined by the vector that connects that point to the remaining points; the translation vector. A “translations plot” is generated by superimposing the sets of points at the ends of the translation vectors for every point on a common origin (e.g. Figure 5b). The translations plot shows alignments of points and characteristic spacings between such alignments. The plot commonly reveals patterns and trends that are not visible simply from examining the distribution of the point centres themselves, partly because the number of points on the translations plot is given by n^2-n from n original data points. Consequently the method is particularly useful for data sets that have few data points. The orientation of the translations vectors can be represented and analysed further through the use of rose diagrams (e.g. Figure 5c). However, it is important to appreciate that there is no absolute location for the translations plot; it is based on relative positions. The method can also be applied in three dimensions to produce a three-dimensional translations plot.

Fry analyses performed during this study utilised computer programs written specifically for this project by Dr. T. G. Blenkinsop.

The application of Fry analysis to Bendigo

The spatial analysis of historical production from workings within the Bendigo Goldfield has been carried out using shaft and level production data, which was supplied by BML. Two databases have been generated (Appendix D) from the historical data. The first contains X and Y co-ordinates, relative to mine grid, for a total of 169 shaft collars (Figure 5a) for which tonnage-weighted head grades have been calculated. The second database is comprised of underground production data and three-dimensional co-ordinates for 864 point localities, which are located within the 169 shafts and adjoining levels. Importantly, any spatial variability between the reported

production data and in-situ mineralisation is considered to be minimal, given the small mining leases and the close proximity of individual workings (e.g. Figure 4a).

The two- and three-dimensional datasets have been subdivided based on grade in order to examine the effect of grade. The two-dimensional database has been subdivided into 4 grade ranges each containing between 49 and 51 data points (Appendix D). The three-dimensional database has been subdivided into 10 grade ranges each containing between 50 and 130 data points (Appendix D). After applying Fry analysis to each of the subsets the resultant translations were imported into Maptek's Vulcan software, which made it possible to view the data in three-dimensions.

The following two sections demonstrate the existence of previously unrecognised high-grade trends through the use of two- and three-dimensional translations plots and moving average rose diagrams (MARD). MARD have been plotted by taking a 10° moving average, plotted at every degree.

Two-dimensional analysis

The location of the historical shafts (Figure 5a) shows a strong NNW-SSE alignment that coincides with the axial traces of F₂ anticlines (Figure 3).

The highest-grade interval defined for the two-dimensional shaft data is 17.8 to 193 g/t and comprises 51 shafts. The resulting translations plot consists of 2550 translations and is shown in Figure 5b. The corresponding MARD (Figure 5c) shows, as expected, the dominant high-grade trend is orientated NNW-SSW (T1). However, a secondary trend (T2) orientated NW-SE is also apparent. In order to reduce the dominance of the NNW-SSE trend and enhance the presence of any subordinate trends, two subsequent MARD have been plotted for translations within 5km and 2km respectively (Figure 5c). The MARD for translations within 5km confirms the presence of T2, but reveals the existence of another, less prominent secondary trend (T3) that strikes NE-SW. The MARD for translations within 2km demonstrates that the T2 and T3 trends are in fact comprised of five secondary high-grade trends (T2a, T2b, T2c, T3a and T3b). The relative magnitudes of the secondary trends are as follows: T2a ≥ T2b > T3a > T3b > T2c. Bearings for the six high-grade trends are presented in Table 1.

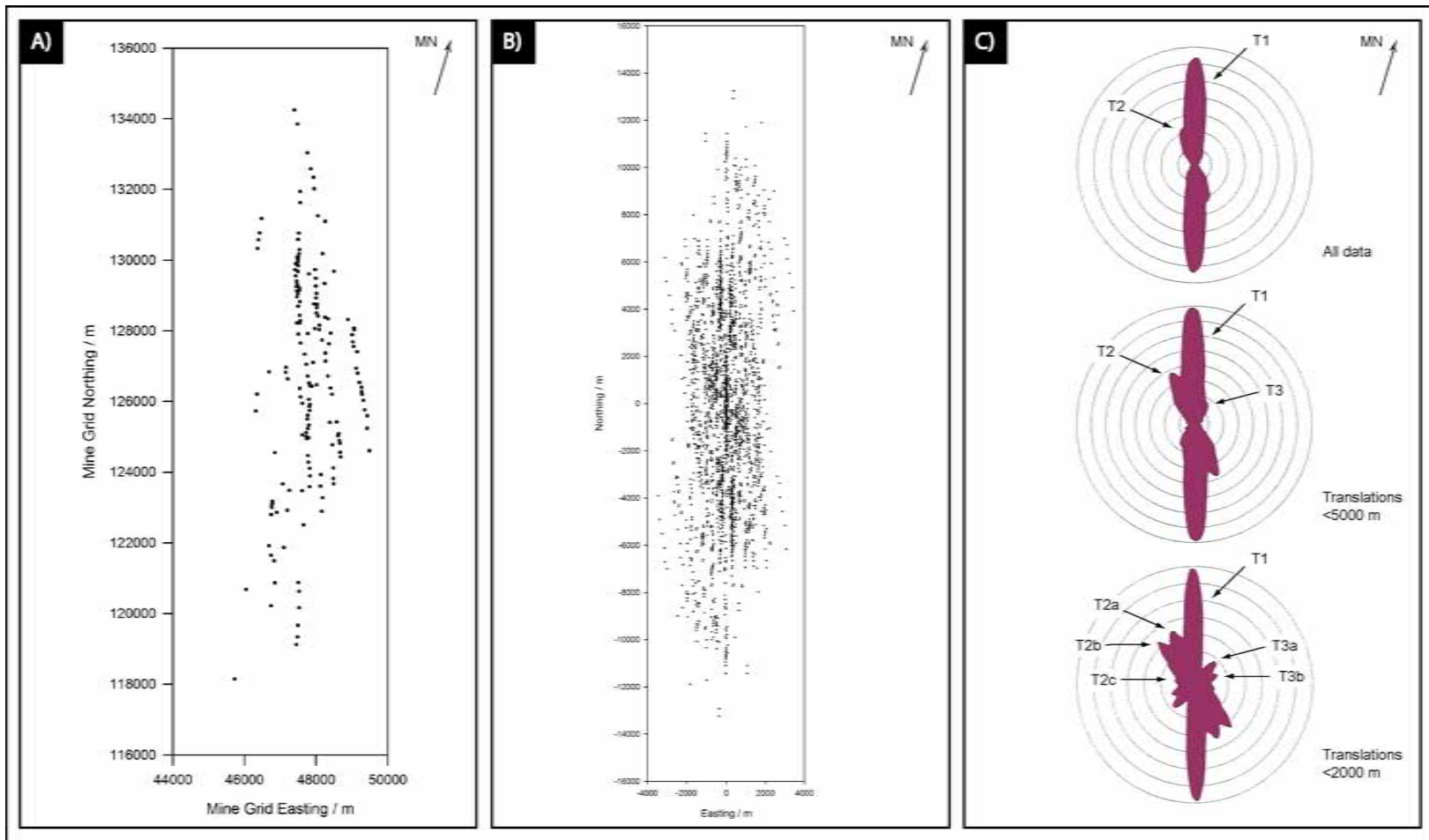


Figure 5. A Distribution of historical shaft collars. $N = 169$. B. Translations for grade range 17.8-193 g/t. $N = 2550$. C. Corresponding MARD for translations vectors.

Table 1. Bearings for high-grade trends determined for two-dimensional data with a grade range 17.8 g/t to 193 g/t.

Trend	T1	T2a	T2b	T2c	T3a	T3b
Bearing relative to magnetic north	344°	323°	306°	276°	033°	061°

The spatial analysis of data from the three remaining grade ranges (0.0 to 9.3 g/t; 9.4 to 14.4 g/t and 14.5 to 25.4 g/t; Appendix D) has revealed comparable grade trends to those identified above (Figure 5c; Table 2). However, despite the similarities between the translations plots and MARD for each of the four grade ranges (Appendix D) there are two apparent differences. The first involves a reversal in the relative magnitudes of the T2 and T3 trends, whereby T3 trends become more significant than T2 trends as grade decreases. The second difference is that the lower grade ranges are characterised by an increased variability in the orientation of T1 (Appendix D).

The similar trends observed for each of the four grade ranges indicates that grade only has a limited influence on the trends within the two-dimensional production data. The consistency in the grade trends also suggests that the same structures controlled the localisation of both high and low grade mineralisation.

Three-dimensional analysis

The spatial distribution of three-dimensional production data strongly reflects the NNW-SSE trending F_2 folds, regardless of grade. The data also emphasises the density and vertical extent of the workings within the goldfield (Figure 6a, b).

Although the three-dimensional data has been subdivided in to 10 grade ranges (Appendix D), well defined three-dimensional grade trends other than T1 may only be observed when analysing data from the highest-grade range.

The highest-grade interval defined for the three-dimensional data is 45 to 733 g/t and consists of 52 data points from various shafts (Appendix D). In plan view, the corresponding translations plot, which comprises 2652 points, is characterised by one dominant and three subordinate high-grade trends (Figure 6c, d, e, f). The dominant trend is orientated NNW-SSE, parallel to the F_2 folds (T1). The three secondary trends correspond to T2a, T2b and T3a as defined from the two-dimensional data; T2c and T3b

are absent (Figure 6c, f). When the translations plot is viewed in a vertical plane orthogonal to T2a, a trend with a shallow plunge towards NE is evident (Figure 6d). In a view of the translations plot in a vertical plane orthogonal to T2b, a strong trend with a moderate plunge towards NNE can be observed (Figure 6e). It is suggested that T2a and T2b are linear trends (Figure 6d, e; Table 2) and that it is an alignment of these linear trends that defines T2a and T2b as observed in plan view (Figure 6c, f). A trend conforming to T3a was not readily observable. A high-grade trend similar to T2a was observed in assay data from underground drilling (Figure 6g), but this is not discussed further due to the sensitive nature of the data.

The most prominent high-grade trend (T1; Table 2; Figure 5c) is coincident with the strike of D₂ folds and faults, reflecting the strong control that these structures had on the localisation of auriferous mineralisation. The T2 and T3 trends (Table 2; Figures 5c & 6), which have not previously been recognised, are prominent for translations within 2km, which implies that the structural controls on these high-grade trends occur both at a goldfield and deposit scale. The high-grade trends recognised using the technique of Fry analysis are summarised in Table 2.

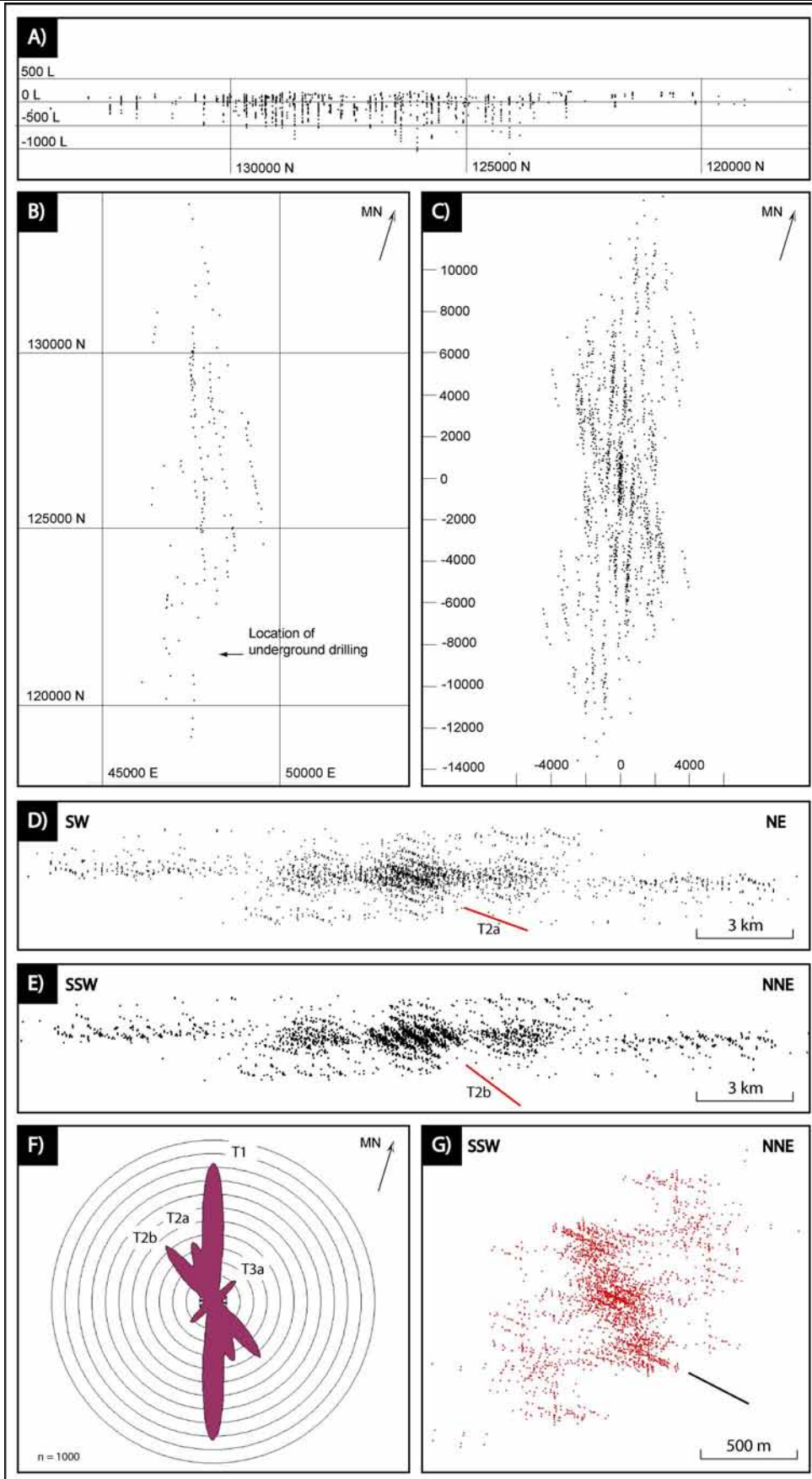


Figure 6. A. Vertical longitudinal section showing the vertical extent of the three-dimensional historical production data. $N = 864$. B. Location of the shafts for which the three-dimensional production data corresponds. $N = 169$. The location of current underground drilling by Bendigo Mining is shown. C. Translations plot for grade range 45 to 733 g/t. $N = 2652$. D. Vertical section perpendicular to trend T2a. The shallow plunging T2a trend is clearly visible. E. Vertical section perpendicular to trend T2d. The moderately plunging T2b trend is very strong. F. Corresponding MARD for translations <2000 m. The dominant trends correspond to those recognised in the two-dimensional study; with the exception that trend T2c and T3b are absent. G. Translations plot for high-grade drill intersection at Bendigo Mining Ltd. Note the strong trend that has a similar plunge to trend T2a.

Table 2. Summary of high-grade trends observed in two- and three-dimensional translations plots. It was not possible to quantify the three-dimensional direction of the high-grade trends.

High Grade Trend		Bearing	Plunge	Plunge Direction
T1		344°	Vertical	-
T2	T2a	146°	NE	Shallow
	T2b	126°	NNE	Moderate
	T2c	096°	-	-
T3	T3a	033°	-	-
	T3b	061°	-	-

Ore shoot geometry and location

It is widely reported that the majority of economic gold occurrences within the Bendigo Goldfield are associated with D_2 quartz veins situated within or proximal to F_2 hinge zones (e.g. Dunn, 1896; Whitelaw, 1914; Stillwell, 1922, 1950, 1953; Herman, 1923; Stone, 1937; Chace, 1949; Thomas, 1953a, b; Wilkinson, 1988b; Forde, 1989; Sharpe & MacGeehan, 1990; Cox *et al.*, 1991a; Willman & Wilkinson, 1992; Jia *et al.*, 2000; Johansen, 2001b; Schaub & Wilson, 2002; Sections A & C). The significance of the relationship between F_2 hinge zones and auriferous mineralisation is clearly emphasised by the dominance of the T1 trend. However, it has been demonstrated that economic gold occurrences formed not during D_2 , but during D_3 (Section C) and are therefore only spatially related to the F_2 hinge zones and D_2 quartz veins. This spatial relationship, which is represented by the T1 trend, supports the view that deformation

associated with D_3 exploited the competency contrast between the host rock and D_2 quartz veins (Section C), and suggests that the auriferous fluids exploited some of the same fluid pathways (e.g. Cox *et al.*, 1991a; Schaub & Wilson, 2002; Schaub and Zhao, 2002) as the preceding D_2 quartz phases, with gold being precipitated at a similar structural level. Although economic gold occurrences were deposited proximal to earlier mineral phases (Section C), both laterally and vertically, it may have been the D_3 structures that controlled the along strike occurrence of gold and ore shoot geometry.

The T2 and T3 trends (Table 2) do not coincide with the orientation of D_3 kink band axial surfaces, but are instead coincident with the intersection axes between S_0 and S_3 (Figure 7) and in a few instances, S_2 and S_3 . This implies that it is the intersection of D_3 kink bands with bedding and bedding parallel structures (e.g. D_2 quartz veins and faults) that controls the plunge and plunge direction of ore shoots. Furthermore, the plunge and plunge direction of the T2 trends (Table 2) is comparable with the ore shoots measured by Whitelaw (1914) and more recently, those encountered by Bendigo Mining Ltd (see Figure 6g).

The reversal in the relative magnitudes of the T2 and T3 trends with decreasing grade indicates that the T2 trends represent the richest ore shoots. The orientation of the T2 trends (Table 2; Figure 7) is coincident with the intersection axes between NE-NW dipping kink band axial surfaces and bedding or bedding parallel structures. This suggests that it is the D_3 kink bands with orientations comparable to S_{3b} and S_{3c} (Figure 7; Sections A & B) that host the most economically significant mineralisation within the goldfield. This in turn corresponds to historical reports on the central portion of the field, which state that the most significant high-grade mineralisation was intersected on north plunging F_2 folds (e.g. Whitelaw, 1914; Stone, 1937).

It is proposed that the location of high-grade zones within the Bendigo Goldfield is related to F_3 kink bands and in particular the kink band axial surfaces (e.g. Figure 3c). It is also proposed that the orientation of ore shoots conform to the intersection axes between F_3 axial surfaces and D_2 quartz veins, which also appears to be the case where zones of intense S_3 (higher strain) intersect D_2 quartz veins (Figure 8). These zones of higher strain almost always occur within F_3 kink bands and may explain the occurrence of high-grade shoots distal to F_3 axial planes.

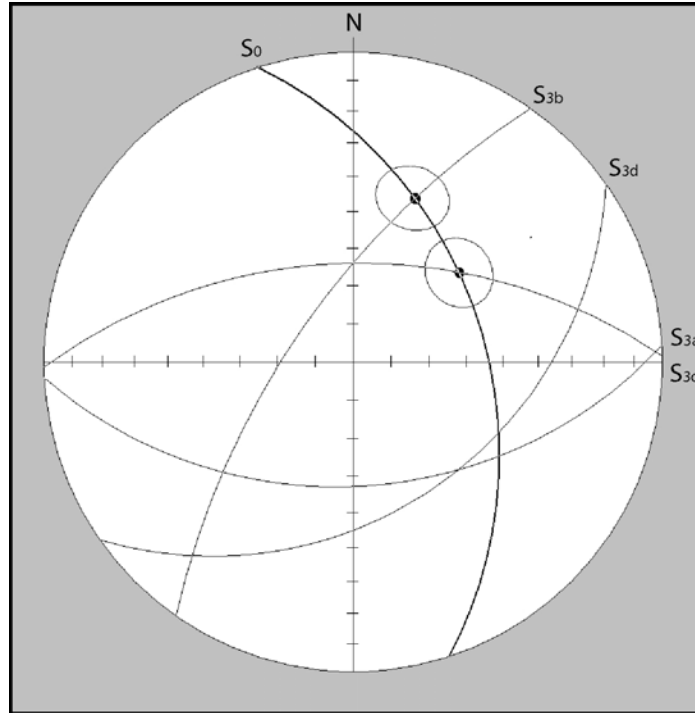


Figure 7. Lower hemisphere equal area stereonet showing S_{3a} , b , c , d as observed in sample G131, Garrard's Reef. An error of $\pm 9^\circ$ is associated with the orientation of S_3 and is represented by the circle encompassing the intersection axes (See Sections A & B). It must also be noted that the dip and dip direction of bedding may vary and that a generalised orientation has been plotted. The intersection of bedding with S_{3b} and S_{3c} gives intersection axes of 42° towards 020° and 51° towards 051° respectively. Although the intersection axes defined here are slightly steeper than the T2 trends reported in Table 2, their orientation is comparable.



Figure 8. A & B. Photographs showing the eastern margin of the D3 leg reef. Two sets of well-developed L_2^3 intersection lineations, one set pitching north (L1) and one set south (L2), are clearly visible on the hangingwall. Visible gold, marked by yellow and pink dots, and pink circles, only occur where D_2 quartz has been reactivated proximal to the vein margin. The occurrence of L_2^3 intersection lineations defines a zone of high strain, which corresponds to the occurrence of gold (see Figure 10e). D3 Leg reef, Deborah Anticline. View to the east and northeast respectively.

IMPLICATIONS FOR NEAR MINE EXPLORATION

The structural evolution of the Bendigo goldfield, the relative timing of gold and the controls on gold localisation have been a matter of contention (e.g. Chace, 1949; Thomas, 1953a; Forde, 1989; Schaub & Wilson, 2002; Sections A, B & C). To enhance the predictive capabilities of current exploration protocols the following section builds on a revised deformation chronology (Sections A & B), a syn- D_3 timing for gold (Section C) and a new model for gold localisation (this section).

The identification of prospective areas within the Bendigo region relies on four key features:

1. The vertical repetition of D_2 structures possibly due to a lithological control;
2. The presence of D_2 folds and deposit scale faults;
3. The presence of D_2 quartz veins (e.g. fault related veins) proximal to F_2 anticlinal hinge zones; and
4. The presence of D_3 kink bands.

Within the goldfield highly prospective areas for economic mineralisation correspond to the location of kilometre-scale F_3 kink bands (Figure 3; Sections A & B) and in particular the F_3 axial surfaces (e.g. Figure 3c). An area defined by an absence of kilometre-scale F_3 kink bands does not rule out the existence of significant high-grade mineralisation. On the contrary, an F_3 kink band with a strike length of several hundred metres may host extensive mineralisation, particularly given the proximity of the two axial surfaces. A complete absence of any F_3 kink bands may be viewed as discouraging.

The demarcation of F_3 kinks requires detailed structural mapping, both on surface and underground. However, within the goldfield two obvious problems exist:

1. A lack of outcrop due to urban development, and

2. The lozenge form of a kink band (Weiss, 1968) means that there is a critical kink band width, whereby the minimum vertical extent of that kink band may not extend below the lower limit of historical stoping.

There may also be F_3 kink bands at depth that have no surface expression on the current topographic plane.

Three-dimensional models have been constructed of the F_3 kink bands using Maptek's Vulcan software (Figure 9). The location of the kink bands is based on a reinterpretation of the 1:10,000 geological maps (Willman & Wilkinson, 1992) and the vector analysis of F_2 axial traces (Sections A & B). It has been assumed that the axial surfaces are planar and of constant dip (50°). The dip direction of kink band axial surfaces has been determined from the plunge direction of F_2 within the respective kink band (see Figure 4b in Section B).

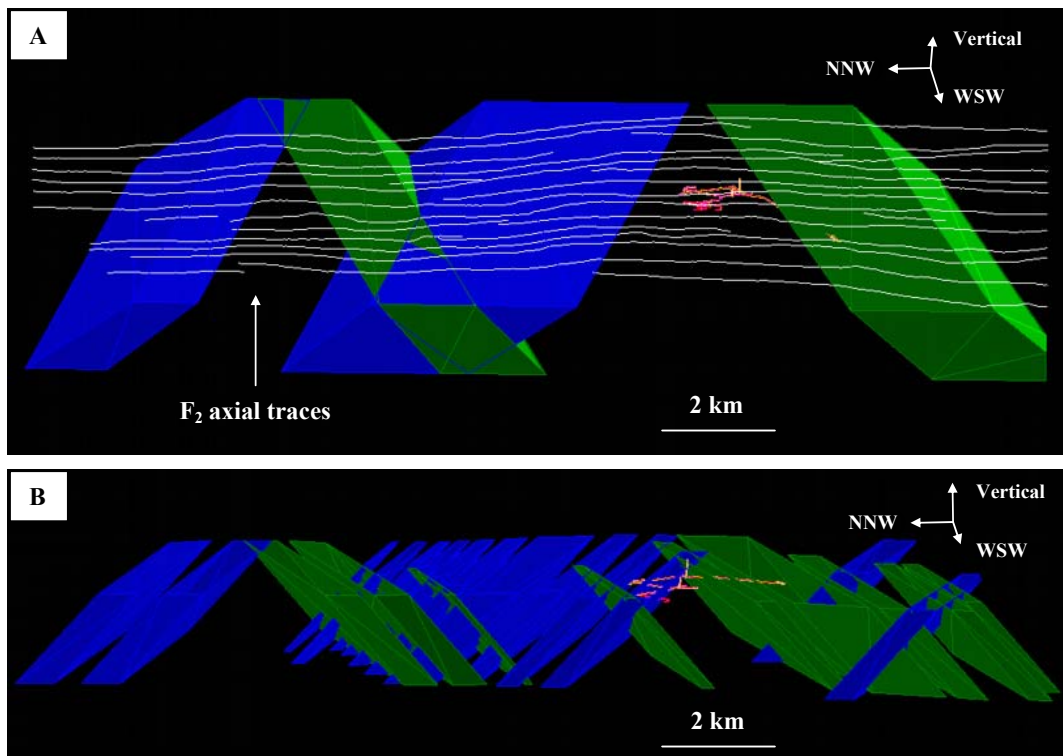


Figure 9. A. The orientation of kilometre-scale F_3 kink bands, which strongly influence the architecture of the goldfield. The blue kinks have a sinistral sense, whereas the green kinks have a dextral sense. Current underground mine development, including the Swan decline and on-lode development, is shown. B. Detailed model of F_3 kink bands within the limits of the goldfield. The blue kinks have a sinistral sense, whereas the green kinks have a dextral sense. Current underground mine development, including the Swan decline and on-lode development, is shown. Both models have been rotated slightly about a horizontal NNW-SSE trending axis.

In Figure 9a the kilometre-scale F_3 kink bands delineate large-scale simultaneous changes in the strike and plunge of F_2 . The largest of the F_3 kink bands has a sinistral sense and north dipping axial surfaces. Figure 9b is a more detailed interpretation of the F_3 kink bands and shows the centre of the goldfield to be characterised by a high density of north dipping sinistral kink bands, within which the F_2 folds plunge northwest. This corresponds with the results from the spatial analysis of historical production data (see above) and historical reports on the central portion of the field, which state that significant high-grade mineralisation was intersected on north plunging F_2 folds (e.g. Whitelaw, 1914; Stone, 1937; Figure 3).

Once D_3 kink bands have been identified on a scale such as that shown in Figure 9b, two scenarios exist. The first is that the F_3 kink bands are distal to current development. In such instances an F_3 kink band is best treated as a target for future exploration when underground development becomes proximal. The integration of distal F_3 kink bands with the ribbon repeat model (see Johansen, 2001b) is potentially a powerful tool for identifying future target zones.

If the F_3 kink band is deemed to be of significant interest an exploration program could be initiated to investigate D_2 structures and quartz bodies proximal to the kink band. However, this is an unlikely option given the depth of potential targets and the costs involved in extending exploration drives to provide underground drilling platforms.

The second and most important scenario is that an F_3 kink band either intersects or is proximal to the current mine development. In such instances the reliance on surface outcrop to define kink band geometry is greatly reduced. Structural measurements from orientated drill core, underground mapping of exploration development and detailed three-dimensional modelling of stratigraphy would enable a detailed geometric analysis of the kink band. The benefit of carrying this analysis out from remote development is that F_3 kink bands can be extrapolated to the anticlinal hinge zones, both laterally and vertically, thus defining potential deposit-scale targets on a number of adjacent anticlines. Exploration for D_2 quartz veins is fundamental because inevitably it is the intersection of D_3 kink bands with D_2 quartz veins that dictates ore shoot location and orientation.

It is also important to investigate zones of higher D_3 strain, which almost always occur within F_3 and are defined by the occurrence of intense S_3 (e.g. Figure 8; Section A). The

F₂ folds that host the auriferous quartz reefs currently exposed in underground development have a general plunge to the north-northwest, which locally exceeds 20°. Furthermore, the identification of NNW pitching ore shoots (*pers. comm.* S. Dominy, 2005; Figure 6g) suggests that the auriferous mineralisation is controlled by D₃ kink bands (Figure 9b). Zones of higher D₃ strain have been mapped within the current development and the intensity of deformation scaled according to the width of S₃ intersection lineations (Figures 10). A potential problem encountered was that two S₃ intersection lineations were almost always present within zones of higher D₃ strain. This implies that the strike of a high strain zone is not necessarily parallel to the host F₃ kink band. To resolve this, high strain zones need to be traced laterally to obtain their strike (i.e. across a drive or between drives).

A comparison between the intensity of D₃ deformation and the grade of on-lode development shows a positive correlation (Figure 10). Although there is good correlation between the intensity of D₃ deformation and grade, it is apparent that the relationship between the intensity of deformation and visible gold is much stronger (e.g. Figure 8). The occurrence of S₃, whether in drill core or in outcrop can be considered as a proxy for gold and in the case of the latter, S₃ is apparently fundamental to ore shoot location and orientation within the D₂ quartz reefs.

For exploration to be successful within the Bendigo Goldfield an integrated approach must be taken. Exploration is scale dependant and requires a strong understanding of the structural controls on mineralisation. At a goldfield scale, exploration requires the delineation of F₃ kink bands (e.g. Figure 9), which when combined with the ribbon repeat model and historical production data, is a powerful tool for defining blind targets. At a deposit scale, a refinement in the demarcation of F₃ kink bands, integrated with the ribbon repeat model, diamond drilling, underground development and detailed geological studies is fundamental for predicting the location of economic mineralisation. The identification that D₃ kink bands control ore shoot location and orientation significantly enhances the current exploration strategy and improves exploration potential within the goldfield. The scale of kink bands outlined in Figure 9 suggests that significant mineralisation may be present at depth.

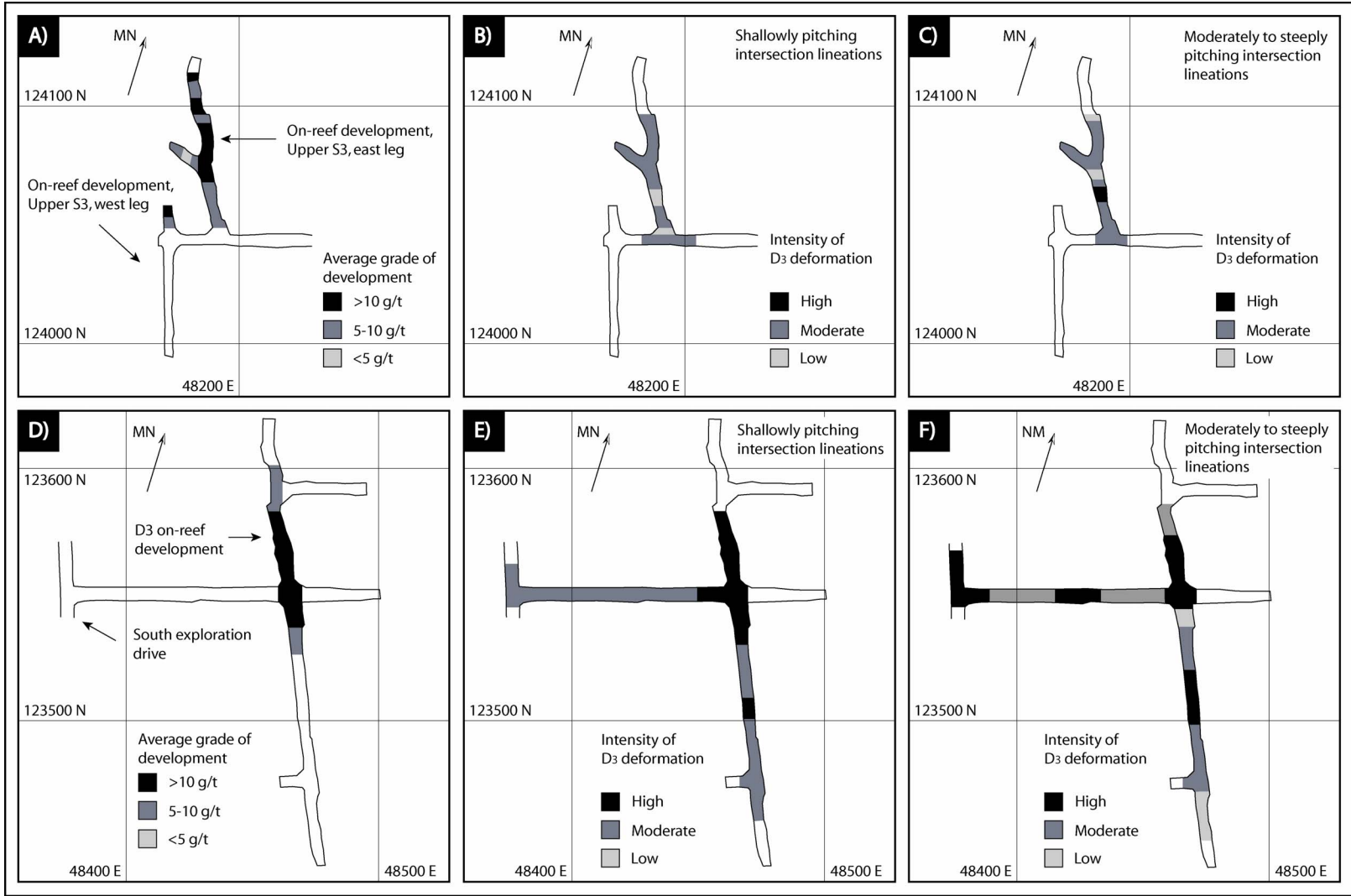


Figure 10. A. Simplified grade distribution for on-lode development on the Upper S3 saddle reef. B. Intensity of deformation associated with shallow pitching L_2^3 intersection lineations. Upper S3 saddle reef. C. Intensity of deformation associated with moderately to steeply pitching L_2^3 intersection lineations. Upper S3 saddle reef. D. Simplified grade distribution for on-lode development on the D3 leg reef. E. Intensity of deformation associated with shallow pitching L_2^3 intersection lineations. D3 leg reef. F. Intensity of deformation associated with moderately to steeply pitching L_2^3 intersection lineations. D3 leg reef. Scale defining intensity of D_3 deformation: Low – intersection lineations less than 0.5 mm in width; Medium – intersection lineations between 0.5 mm and 1.5mm in width; High – intersection lineations more than 1.5mm in width.

CONCLUSIONS

1. Areas of the goldfield characterised by significant historical production coincide with F_3 kink bands and in particular, F_3 axial traces (e.g. Figure 3c)
2. High-grade trends in historical production data indicate that it is the intersection of F_3 axial planes with bedding and bedding parallel structures that controls ore shoot location and geometry.
3. On a reef-scale, zones of intense D_3 deformation have a positive correlation with economic grades. It is suggested that these zones of high strain control the orientation and location of ore shoots within F_3 .
4. The identification of the structural controls on ore shoot location and geometry has considerable implications for resource evaluation. It also emphasises the need for structural data and interpretation in the resource estimation process.
5. The current exploration strategy needs to incorporate the structural model for D_3 kink bands, which combined with the ribbon repeat model, diamond drilling and underground development would significantly improve exploration success within the goldfield.
6. In terms of diamond drilling, orientated core is a necessity. The orientation of S_0 , S_1 and S_2 , combined with the plunge and plunge direction of F_2 will inevitably aid the demarcation of F_3 . The recognition of F_3 also benefits the exploration drilling program by providing a tighter constraint on potential target zones.
7. The revised model for exploration may have implications for exploration both within and proximal to other central Victorian goldfields.